











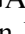












## Disequilibrium oxygen isotope distribution among aqueously altered minerals in Ryugu asteroid returned samples

Noriko T. KITA <sup>1,\*</sup>, Kouki KITAJIMA<sup>1</sup>, Kazuhide NAGASHIMA <sup>2</sup>, Noriyuki KAWASAKI <sup>3</sup>, Naoya SAKAMOTO<sup>4</sup>, Wataru FUJIYA <sup>5</sup>, Yoshinari ABE<sup>6</sup>, Jérôme ALÉON <sup>7</sup>, Conel M. O'D. ALEXANDER<sup>8</sup>, Sachiko AMARI<sup>9,10</sup>, Yuri AMELIN<sup>11</sup>, Ken-ichi BAJO<sup>3</sup>, Martin BIZZARRO<sup>12</sup>, Audrey BOUVIER <sup>13</sup>, Richard W. CARLSON<sup>8</sup>, Marc CHAUSSIDON<sup>14</sup>, Byeon-Gak CHOI<sup>15</sup>, Nicolas DAUPHAS<sup>16</sup>, Andrew M. DAVIS<sup>16</sup>, Tommaso DI ROCCO<sup>17</sup>, Ryota FUKAI <sup>18</sup>, Ikshu GAUTAM<sup>19</sup>, Makiko K. HABA <sup>19</sup>, Yuki HIBIYA<sup>20</sup>, Hiroshi HIDAKA<sup>21</sup>, Hisashi HOMMA<sup>22</sup>, Peter HOPPE<sup>23</sup>, Gary R. HUSS <sup>2</sup>, Kiyohiro ICHIDA<sup>24</sup>, Tsuyoshi IIZUKA <sup>25</sup>, Trevor R. IRELAND<sup>26</sup>, Akira ISHIKAWA<sup>19</sup>, Shoichi ITOH<sup>27</sup>, Thorsten KLEINE<sup>28</sup>, Shintaro KOMATANI<sup>24</sup>, Alexander N. KROT <sup>2</sup>, Ming-Chang LIU<sup>29,30</sup>, Yuki MASUDA <sup>19</sup>, Kevin D. MCKEEGAN<sup>29</sup>, Mayu MORITA<sup>24</sup>, Kazuko MOTOMURA<sup>31</sup>, Frédéric MOYNIER<sup>14</sup>, Izumi NAKAI<sup>32</sup>, Ann NGUYEN <sup>33</sup>, Larry NITTLER<sup>8</sup>, Morihiko ONOSE<sup>24</sup>, Andreas PACK<sup>17</sup>, Changkun PARK <sup>34</sup>, Laurette PIANI<sup>35</sup>, Liping QIN<sup>36</sup>, Sara S. RUSSELL <sup>37</sup>, Maria SCHÖNBÄCHLER <sup>38</sup>, Lauren TAFLA<sup>29</sup>, Haolan TANG<sup>29</sup>, Kentaro TERADA<sup>39</sup>, Yasuko TERADA<sup>40</sup>, Tomohiro USUI<sup>18</sup>, Sohei WADA<sup>3</sup>, Meenakshi WADHWA<sup>41</sup>, Richard J. WALKER <sup>42</sup>, Katsuyuki YAMASHITA<sup>43</sup>, Qing-Zhu YIN<sup>44</sup>, Tetsuya YOKOYAMA<sup>19</sup>, Shigekazu YONEDA<sup>45</sup>, Edward D. YOUNG <sup>29</sup>, Hiroharu YUI<sup>46</sup>, Ai-Cheng ZHANG <sup>47</sup>, Tomoki NAKAMURA<sup>48</sup>, Hiroshi NARAOKA <sup>49</sup>, Takaaki NOGUCHI <sup>27</sup>, Ryuji OKAZAKI<sup>49</sup>, Kanako SAKAMOTO<sup>18</sup>, Hikaru YABUTA<sup>50</sup>, Masanao ABE<sup>18</sup>, Akiko MIYAZAKI<sup>18</sup>, Aiko NAKATO<sup>18</sup>, Masahiro NISHIMURA<sup>18</sup>, Tatsuaki OKADA<sup>18</sup>, Toru YADA<sup>18</sup>, Kasumi YOGATA<sup>18</sup>, Satoru NAKAZAWA<sup>18</sup>, Takanao SAIKI<sup>18</sup>, Satoshi TANAKA<sup>18</sup>, Fuyuto TERUI<sup>51</sup>, Yuichi TSUDA<sup>18</sup>, Sei-ichiro WATANABE<sup>21</sup>, Makoto YOSHIKAWA<sup>18</sup>, Shogo TACHIBANA <sup>52</sup>, and Hisayoshi YURIMOTO <sup>3,4</sup>

<sup>1</sup>WiscSIMS, Department of Geoscience, University of Wisconsin-Madison, Madison, Wisconsin, USA

<sup>2</sup>Hawai'i Institute of Geophysics and Planetology, University of Hawai'i at Mānoa, Honolulu, Hawaii, USA

<sup>3</sup>Department of Natural History Sciences, Hokkaido University, Sapporo, Japan

<sup>4</sup>Isotope Imaging Laboratory, Creative Research Institution, Hokkaido University, Sapporo, Japan

<sup>5</sup>Faculty of Science, Ibaraki University, Mito, Japan

<sup>6</sup>Graduate School of Engineering Materials Science and Engineering, Tokyo Denki University, Tokyo, Japan

<sup>7</sup>Institut de Minéralogie, de Physique des Matériaux et de Cosmochimie, Sorbonne Université, Museum National d'Histoire Naturelle, Centre National de la Recherche Scientifique Unité Mixte de Recherche 7590, IRD, Paris, France

<sup>8</sup>Earth and Planets Laboratory, Carnegie Institution for Science, Washington, DC, USA

<sup>9</sup>McDonnell Center for the Space Sciences and Physics Department, Washington University, St. Louis, Missouri, USA

<sup>10</sup>Geochemical Research Center, The University of Tokyo, Tokyo, Japan

<sup>11</sup>Guangzhou Institute of Geochemistry, Chinese Academy of Sciences, Guangzhou, China

<sup>12</sup>Centre for Star and Planet Formation, Globe Institute, University of Copenhagen, Copenhagen K, Denmark

<sup>13</sup>Bayerisches Geoinstitut, Universität Bayreuth, Bayreuth, Germany

<sup>14</sup>Institut de Physique du Globe de Paris, Centre National de la Recherche Scientifique, Université Paris Cité, Paris, France

<sup>15</sup>Department of Earth Science Education, Seoul National University, Seoul, Republic of Korea

<sup>16</sup>Department of the Geophysical Sciences and Enrico Fermi Institute, The University of Chicago, Chicago, Illinois, USA

<sup>17</sup>Faculty of Geosciences and Geography, University of Göttingen, Göttingen, Germany

<sup>18</sup>Institute of Space and Astronautical Science, Japan Aerospace Exploration Agency, Sagami, Japan

<sup>19</sup>Department of Earth and Planetary Sciences, Tokyo Institute of Technology, Tokyo, Japan

<sup>20</sup>Research Center for Advanced Science and Technology, The University of Tokyo, Tokyo, Japan

<sup>21</sup>Department of Earth and Planetary Sciences, Nagoya University, Nagoya, Japan

<sup>22</sup>Osaka Application Laboratory, Rigaku Corporation, Osaka, Japan

- <sup>23</sup>Max Planck Institute for Chemistry, Mainz, Germany
- <sup>24</sup>Analytical Technology, Horiba Techno Service Co. Ltd., Kyoto, Japan
- <sup>25</sup>Department of Earth and Planetary Science, The University of Tokyo, Tokyo, Japan
- <sup>26</sup>School of Earth and Environmental Sciences, The University of Queensland, St. Lucia, Qld, Australia
- <sup>27</sup>Division of Earth and Planetary Sciences, Kyoto University, Kyoto, Japan
- <sup>28</sup>Max Planck Institute for Solar System Research, Göttingen, Germany
- <sup>29</sup>Department of Earth, Planetary, and Space Sciences, University of California, Los Angeles, Los Angeles, California, USA
- <sup>30</sup>Lawrence Livermore National Laboratory, Livermore, California, USA
- <sup>31</sup>Thermal Analysis, Rigaku Corporation, Tokyo, Japan
- <sup>32</sup>Department of Applied Chemistry, Tokyo University of Science, Tokyo, Japan
- <sup>33</sup>Astromaterials Research and Exploration Science Division, National Aeronautics and Space Administration Johnson Space Center, Houston, Texas, USA
- <sup>34</sup>Division of Earth-System Sciences, Korea Polar Research Institute, Incheon, Republic of Korea
- <sup>35</sup>Centre de Recherches Pétrographiques et Géochimiques, Centre National de la Recherche Scientifique–Université de Lorraine, Nancy, France
- <sup>36</sup>School of Earth and Space Sciences, University of Science and Technology of China, Hefei, Anhui, China
- <sup>37</sup>Department of Earth Sciences, Natural History Museum, London, UK
- <sup>38</sup>Institute for Geochemistry and Petrology, Department of Earth Sciences, Eidgenössische Technische Hochschule Zürich, Zürich, Switzerland
- <sup>39</sup>Department of Earth and Space Science, Osaka University, Osaka, Japan
- <sup>40</sup>Spectroscopy and Imaging, Japan Synchrotron Radiation Research Institute, Hyogo, Japan
- <sup>41</sup>School of Earth and Space Exploration, Arizona State University, Tempe, Arizona, USA
- <sup>42</sup>Department of Geology, University of Maryland, College Park, Maryland, USA
- <sup>43</sup>Graduate School of Natural Science and Technology, Okayama University, Okayama, Japan
- <sup>44</sup>Department of Earth and Planetary Sciences, University of California, Davis, Davis, California, USA
- <sup>45</sup>Department of Science and Engineering, National Museum of Nature and Science, Tsukuba, Japan
- <sup>46</sup>Department of Chemistry, Tokyo University of Science, Tokyo, Japan
- <sup>47</sup>School of Earth Sciences and Engineering, Nanjing University, Nanjing, China
- <sup>48</sup>Department of Earth Science, Tohoku University, Sendai, Japan
- <sup>49</sup>Department of Earth and Planetary Sciences, Kyushu University, Fukuoka, Japan
- <sup>50</sup>Earth and Planetary Systems Science Program, Hiroshima University, Higashi-Hiroshima, Japan
- <sup>51</sup>Kanagawa Institute of Technology, Atsugi, Japan
- <sup>52</sup>UTokyo Organization for Planetary and Space Science, University of Tokyo, Tokyo, Japan

**\*Correspondence**

Noriko T. Kita, WiseSIMS, Department of Geoscience, University of Wisconsin-Madison, Madison, WI 53706, USA.  
Email: [kita@wisc.edu](mailto:kita@wisc.edu)

(Received 06 July 2023; revision accepted 12 March 2024)

**Abstract**—Oxygen 3-isotope ratios of magnetite and carbonates in aqueously altered carbonaceous chondrites provide important clues to understanding the evolution of the fluid in the asteroidal parent bodies. We conducted oxygen 3-isotope analyses of magnetite, dolomite, and breunnerite in two sections of asteroid Ryugu returned samples, A0058 and C0002, using a secondary ion mass spectrometer (SIMS). Magnetite was analyzed by using a lower primary ion energy that reduced instrumental biases due to the crystal orientation effect. We found two groups of magnetite data identified from the SIMS pit morphologies: (1) higher  $\delta^{18}\text{O}$  (from 3‰ to 7‰) and  $\Delta^{17}\text{O}$  ( $\sim 2\text{‰}$ ) with porous SIMS pits mostly from spherulitic magnetite, and (2) lower  $\delta^{18}\text{O}$  ( $\sim -3\text{‰}$ ) and variable  $\Delta^{17}\text{O}$  (0‰–2‰) mostly from euhedral magnetite. Dolomite and breunnerite analyses were conducted using multi-collection Faraday cup detectors with precisions  $\leq 0.3\text{‰}$ . The instrumental bias correction was applied based on carbonate compositions in two ways, using Fe and (Fe + Mn) contents, respectively, because Ryugu dolomite contains higher amounts of Mn than the terrestrial standard. Results of dolomite and breunnerite analyses show a narrow range of  $\Delta^{17}\text{O}$ ; 0.0‰–0.3‰ for dolomite in A0058 and 0.2‰–0.8‰ for dolomite and breunnerite in C0002. The majority of breunnerite, including large  $\geq 100\ \mu\text{m}$  grains, show systematically lower  $\delta^{18}\text{O}$  ( $\sim 21\text{‰}$ ) than dolomite

(25‰–30‰ and 23‰–27‰ depending on the instrumental bias corrections). The equilibrium temperatures between magnetite and dolomite from the coarse-grained lithology in A0058 are calculated to be  $51 \pm 11^\circ\text{C}$  and  $78 \pm 14^\circ\text{C}$ , depending on the instrumental bias correction scheme for dolomite; a reliable temperature estimate would require a Mn-bearing dolomite standard to evaluate the instrumental bias corrections, which is not currently available. These results indicate that the oxygen isotope ratios of aqueous fluids in the Ryugu parent asteroid were isotopically heterogeneous, either spatially, or temporary. Initial water ice accreted to the Ryugu parent body might have  $\Delta^{17}\text{O} > 2\text{‰}$  that was melted and interacted with anhydrous solids with the initial  $\Delta^{17}\text{O} < 0\text{‰}$ . In the early stage of aqueous alteration, spherulitic magnetite and calcite formed from aqueous fluid with  $\Delta^{17}\text{O} \sim 2\text{‰}$  that was produced by isotope exchange between water ( $\Delta^{17}\text{O} > 2\text{‰}$ ) and anhydrous solids ( $\Delta^{17}\text{O} < 0\text{‰}$ ). Dolomite and breunnerite, along with some magnetite, formed at the later stage of aqueous alteration under higher water-to-rock ratios where the oxygen isotope ratios were nearly at equilibrium between fluid and solid phases. Including literature data,  $\delta^{18}\text{O}$  of carbonates decreased in the order calcite, dolomite, and breunnerite, suggesting that the temperature of alteration might have increased with the degree of aqueous alteration.

## INTRODUCTION

The Hayabusa 2 spacecraft brought back samples from the surface of a C-type (carbonaceous) asteroid, 162173 Ryugu (Tachibana et al., 2022; Watanabe et al., 2019). Samples were collected during the two touch-downs from different landing sites, which were stored in two chambers A and C, respectively, of the Hayabusa spacecraft. Initial analyses of Ryugu samples indicate that they resemble Ivuna-type carbonaceous (CI) chondrites, consisting mainly of minerals that were produced by aqueous alteration in its parent asteroid, such as phyllosilicates, dolomite, magnetite, and pyrrhotite (Ito et al., 2022; Nakamura et al., 2022, 2023; Yokoyama et al., 2023; Yamaguchi et al., 2023). Anhydrous minerals are rare in Ryugu samples, though small mineral fragments of olivine and low-Ca pyroxene were identified, as well as tiny polymineralic fragments, similar to refractory inclusions and chondrules in carbonaceous chondrites (e.g., Kawasaki et al., 2022; Liu et al., 2022; Nakashima et al., 2023).

Oxygen 3-isotope systematics of alteration minerals in carbonaceous chondrites, which are expressed as  $\delta^{17}\text{O}$  and  $\delta^{18}\text{O}$ , per mil (‰) deviation from standard mean ocean water (SMOW; Baertschi, 1976), provide an important tool to understand aqueous activity on their asteroidal parent bodies. Early studies by Clayton and Mayeda (1984) applied carbonate–serpentine oxygen isotope thermometry, where calcite was determined by acid dissolution and matrix separates represent serpentine. They estimated the fluid temperatures of Murchison (CM2) and Orgueil (CI) to be 0 and  $150^\circ\text{C}$ , respectively. Mass-independent fractionations of oxygen 3-isotope in alteration minerals  $\Delta^{17}\text{O}$  ( $=\delta^{17}\text{O}-0.52 \times \delta^{18}\text{O}$ ; Clayton et al., 1991) vary substantially among magnetite,

calcite, and dolomite in carbonaceous chondrites (e.g., Jilly-Rehak et al., 2018; Telus et al., 2019; Tyra et al., 2012; Verdier-Paoletti et al., 2017). Many studies argue that aqueous fluid started with higher  $\Delta^{17}\text{O}$  that decreased with interaction between aqueous fluid and anhydrous minerals with relatively  $^{16}\text{O}$ -poor and  $^{16}\text{O}$ -rich isotope signatures, respectively. There are a limited number of studies on magnetite and carbonates in CI chondrites, especially using in situ techniques, prior to the return of Ryugu samples (e.g., Piralla et al., 2020; Rowe et al., 1994).

Several studies reported in situ oxygen 3-isotope analyses of alteration minerals, magnetite, dolomite, and calcite in Ryugu samples by using secondary ion mass spectrometers (SIMS; Fujiya et al., 2023; McCain et al., 2023; Nagashima et al., 2022; Nakamura et al., 2022; Yokoyama et al., 2023). Yokoyama et al. (2023) and Nagashima et al. (2022) estimated the temperatures of aqueous fluid to be  $37 \pm 10^\circ\text{C}$  and  $92 \pm 21^\circ\text{C}$  using data from co-existing magnetite and dolomite in samples A0058 and C0002, respectively, by applying oxygen isotope thermometry (Zheng, 1991, 1999). Slightly lower temperatures of  $9^{+15}/_{-13}^\circ\text{C}$  and  $20^{+14}/_{-12}^\circ\text{C}$  were estimated using the average oxygen isotope ratios of magnetite and dolomite in samples C0008 and A0022, respectively, by Nakamura et al. (2022). McCain et al. (2023) estimated the temperatures of magnetite–calcite pairs (using fractionation factors of Hayles et al., 2018) in C0009 to be  $0\text{--}20^\circ\text{C}$ . However, magnetite analyses in Ryugu show a significant variation in both  $\delta^{18}\text{O}$  (from  $-11\text{‰}$  to  $+7\text{‰}$ ) and  $\Delta^{17}\text{O}$  (from  $0\text{‰}$  to  $+4\text{‰}$ ), indicating that oxygen isotope ratios of the aqueous fluid in the Ryugu parent asteroid might not be fully equilibrated. Fujiya et al. (2023) conducted C and O isotope analyses of calcite and dolomite in Ryugu and found a larger variation of both  $\delta^{13}\text{C}$  and  $\delta^{18}\text{O}$  in calcite than those in dolomite. They concluded that calcite formed

during prograde alteration over the wide range of temperatures and oxygen fugacity, while dolomite formed during retrograde cooling when aqueous fluid and silicate approached O isotope equilibrium. Analyses of Orgueil and Ivuna CI chondrites generally show similar results to those in Ryugu samples (Fujiya et al., 2023; Piralla et al., 2020; Yokoyama et al., 2023).

In this paper, we further investigate the oxygen 3-isotope systematics of magnetite and carbonates in Ryugu samples using SIMS IMS 1280 at the University of Wisconsin–Madison (WiscSIMS). We employ different analytical approaches compared to previous investigations. For magnetite analyses, the impact energy of primary  $\text{Cs}^+$  ions is reduced from 20 to 13 keV, which is known to improve the reproducibility of instrumental mass fractionations in  $\delta^{18}\text{O}$  from 2 to 3‰ (2SD; standard deviation) to 0.7‰, respectively, caused by the crystal orientation of magnetite (Huberty et al., 2010). Yokoyama et al. (2023) reported the uncertainties of magnetite  $\delta^{18}\text{O}$  analyses to be 2.1‰ based on the reproducibility of a polycrystalline magnetite standard (in 2SD). While the effect is mass dependent and would not affect  $\Delta^{17}\text{O}$  data, analyses of Ryugu magnetite at the higher precisions in  $\delta^{18}\text{O}$  are important for the equilibrium temperature estimates of the aqueous fluid using a magnetite–dolomite pair. For carbonate analyses, we use multi-collection Faraday cups (MCFC) that include the higher gain  $10^{12}$  ohm feedback resistor (e.g., Bouden et al., 2021; Fukuda et al., 2021) for  $^{17}\text{O}$  measurements, which allows us to determine isotope ratios at precisions and accuracy of  $\leq 0.3\text{‰}$  for spot sizes of  $\sim 10\ \mu\text{m}$  (e.g., Fukuda et al., 2022; Siron et al., 2021, 2022; Zhang et al., 2022). In the previous analyses of Ryugu carbonates, electron multiplier (EM) was used for  $^{17}\text{O}$  detection due to low count rates of  $^{17}\text{O}$  ( $< 10^5$  cps) with smaller primary beam sizes ( $\leq 5\ \mu\text{m}$ ; e.g., Yokoyama et al., 2023). The precision and accuracy of isotope ratio analyses using EM are limited to be  $\sim 1\text{‰}$  due to gain stability and counting statistics (e.g., Ushikubo et al., 2012; Yokoyama et al., 2023). Thus, MCFC conditions should be used for the SIMS analyses that require precision and accuracy at  $\leq 0.3\text{‰}$  (e.g., Kita et al., 2009). Furthermore, we use a series of dolomite–ankerite and magnesite–siderite standards for instrumental bias correction in  $\delta^{18}\text{O}$  that significantly change with  $\text{FeCO}_3$  contents (Śliwiński et al., 2016, 2018). The same or a similar set of dolomite–ankerite standards were previously used by Yokoyama et al. (2023), Nagashima et al. (2022), Fujiya et al. (2023), and McCain et al. (2023) for Ryugu dolomite analyses. However, the oxygen isotope ratios of breunnerite in Ryugu have not been determined. The high precision  $\Delta^{17}\text{O}$  analyses of carbonates in Ryugu are compared to bulk Ryugu oxygen isotope ratios (average bulk  $\Delta^{17}\text{O} = 0.60 \pm 0.18$ ,

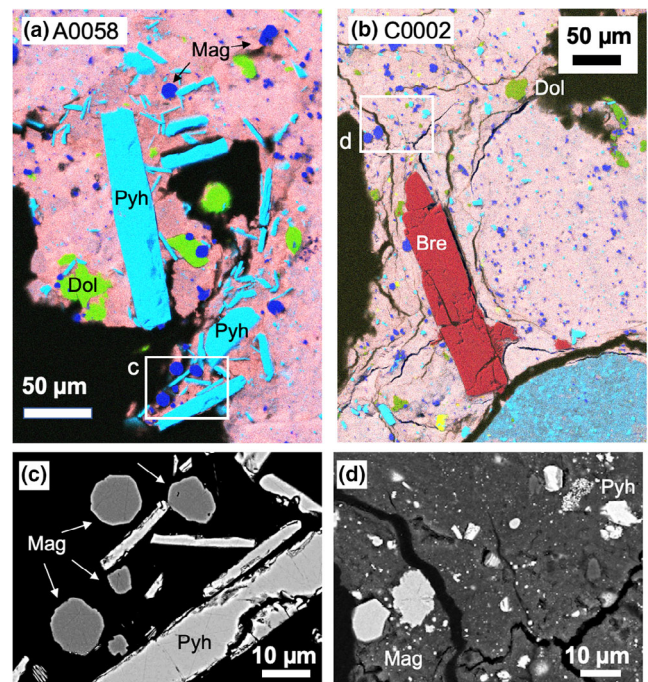


FIGURE 1. Polished sections of Ryugu returned samples. (a) A0058-C1002 pseudocolor x-ray elemental map (RGBgC: Mg-Ca-Fe-Si-S). (b) C0002-C1001 (RGBgCY: Mg-Ca-Fe-Si-S-P). (c) and (d) are BSE images of marked areas in (a) and (b), respectively. Minerals: Mag, magnetite; Pyh, pyrrhotite; Dol, dolomite; Bre, breunnerite.

$n = 15$ ; data from Greenwood et al., 2022; Nakamura et al., 2022; Yokoyama et al., 2023) and further reveal the evolution of aqueous fluid in oxygen three-isotope space.

## METHODS

### Samples

We used two sections of Ryugu A0058-C1002 and C0002-C1001 (Figure 1). A0058-C1002 is the second section of the same sample that was used for SIMS analyses of magnetite and dolomite by Yokoyama et al. (2023). The sample is dominated by a coarse-grained pyrrhotite–magnetite–dolomite assemblage. C0002-C1001 is from the largest particle C0002 among the Ryugu particles reported by Nakamura et al. (2023). The section contains large breunnerite crystals, some of which are  $> 100\ \mu\text{m}$  long, and includes less-altered lithology with olivine and pyroxene that were studied in detail by Kawasaki et al. (2022). Nagashima et al. (2022) analyzed co-existing magnetite and dolomite within an area of  $100\ \mu\text{m}$  across for oxygen 3-isotopes, and Fujiya et al. (2023) analyzed carbon and oxygen 3-isotopes in calcite and dolomite in the same section. Locations of SIMS analyses of magnetite, dolomite, and breunnerite were selected based on x-ray elemental maps and BSE maps of the entire sections that were

prepared at Hokkaido University (Kawasaki et al., 2022; Yokoyama et al., 2023; Figure S1). We selected dolomite and breunnerite grains larger than 15  $\mu\text{m}$  and magnetite grains larger than 5  $\mu\text{m}$ , which do not contain obvious cracks and inclusions. Breunnerite grains are absent in A0058-C1002, so that they were only selected from C0002-C1001. Calcite grains were identified in C0002-C1001 from less-altered areas and were smaller than 10  $\mu\text{m}$  (e.g., Fujiya et al., 2023), so that they were not selected for this study. Major element compositions of dolomite and breunnerite were estimated by using a scanning electron microscope (SEM) with an energy-dispersive x-ray spectroscopy (EDS) detector and used for SIMS instrumental bias correction as described in Yokoyama et al. (2023). Using SEM-EDS was preferred over an electron probe microanalyzer (EPMA) before SIMS measurements to minimize potential beam damage. Carbonate EDS analyses were calibrated using in-house mineral standard (Kawasaki et al., 2022) and SIMS calcite and dolomite standards (Śliwiński et al., 2016, 2018). Molar fractions of  $\text{FeCO}_3$  and  $\text{MnCO}_3$  endmembers of dolomite range 0.03–0.05 and 0.03–0.08, respectively, and those of breunnerite range 0.18–0.33 and 0.02–0.11, respectively (Table S1).

## Secondary Ion Mass Spectrometry

SIMS oxygen 3-isotope analyses of Ryugu samples were conducted by using IMS 1280 at the University of Wisconsin–Madison in two sessions, one for magnetite and another for carbonates, as described below in detail. Raw SIMS data are available in Tables S2 and S3. Additional information is found in Data Repository.

## Carbonate Analyses

The analytical conditions are similar to those of Zhang et al. (2022) for silicate that use multi-collector Faraday cups (MCFC). The primary  $\text{Cs}^+$  ion beam (+10 kV) was set to 1.2 nA in intensity and 10  $\mu\text{m}$  in diameter on the sample surface, and secondary  $^{16}\text{O}^-$  ions were generated; an electron gun was used for charge neutralization. The three isotopes of oxygen were detected simultaneously using two FC detectors on the MC array for  $^{16}\text{O}^-$  and  $^{18}\text{O}^-$  at mass resolving power (MRP, defined as 10% height) of 2200 and on the axial FC detector (FC2) for  $^{17}\text{O}^-$  at MRP = 5000. A single analysis took  $\sim 7$  min, which include 60 s of presputtering, secondary ion beam centering, and the acquisition of signals for 200 s ( $10 \times 20$  cycles). The FC baseline of each detector was monitored during presputtering with a lower-intensity primary beam (50 pA, a few  $\mu\text{m}$  in diameter) rastered over 8  $\mu\text{m}$  square to minimize the sample consumption. The intensity of  $^{16}\text{O}^1\text{H}^-$  was detected at the end of each analysis (using deflector DSP2X), and the tailing correction to  $^{17}\text{O}^-$  signals ( $10 \pm 2$  ppm of  $^{16}\text{O}^1\text{H}^-$ ) was

applied. The gains of the feedback resistors were  $10^{10}$ ,  $10^{12}$ , and  $10^{11}$  ohms for  $^{16}\text{O}^-$ ,  $^{17}\text{O}^-$ , and  $^{18}\text{O}^-$ , respectively. The higher gain  $10^{12}$  ohm resistor provides smaller baseline noise than the  $10^{11}$  ohm resistor (typically  $\sim 160$  cps vs.  $\sim 500$  cps per 60 s integrations, 1SD). Due to a longer time constant for  $10^{12}$  ohm feedback resistor compared to the other resistors ( $\tau \sim 0.74$  s vs.  $\leq 0.1$  s; Fukuda et al., 2021), we applied  $\tau$ -correction (time constant correction) to the  $^{17}\text{O}^-$  signal intensity as a function of the beam growth rate (e.g., Kimura et al., 2016). The growth rate  $g(i)$  at each cycle was estimated from  $^{16}\text{O}$  intensities of three consecutive cycles,  $y(i-1)$ ,  $y(i)$ ,  $y(i+1)$ , using the linear formula  $g(i) = [y(i+1) - y(i-1)]/y(i)/20$  for  $1 < i < 20$ , and  $g(1) = [y(2) - y(1)]/y(1)/10$  and  $g(20) = [y(20) - y(19)]/y(20)/10$  for the first and last cycles, respectively. Then, the tau  $\tau$ -corrected  $^{17}\text{O}$  signal was estimated as  $^{17}\text{O}(i)_{\tau\text{-cor}} = ^{17}\text{O}(i)_{\text{measured}} \times (1 + g(i) \times 0.74)$ .

We used UWC-3 calcite (Kozdon et al., 2009) as the running standard. Typical  $^{16}\text{O}^-$  intensities were  $\sim 2 \times 10^9$  cps. Within a single analysis, both  $\delta^{18}\text{O}_{\text{RAW}}$  and  $\delta^{17}\text{O}_{\text{RAW}}$  drifted to lower values with the depth, which resulted in relatively large internal errors (in 2SE) of 0.6‰ and 0.45‰, respectively. By maintaining nearly constant primary intensities ( $\pm 0.05$  nA), the external reproducibility of UWC-3 calcite running standard was typically 0.2–0.3‰ in 2SD for both  $\delta^{18}\text{O}_{\text{RAW}}$  and  $\delta^{17}\text{O}_{\text{RAW}}$ , which is assigned to be the uncertainty of individual analysis. We define the mass-independent fractionation factor of raw measured ratios as

$$\Delta^{17}\text{O}_{\text{RAW}} = \ln(1 + \delta^{17}\text{O}_{\text{RAW}}/1000) - \beta \ln(1 + \delta^{18}\text{O}_{\text{RAW}}/1000), \quad (1)$$

where  $\beta = 0.528$  is used according to the value commonly used for natural mass-dependent fractionation law in recent literature (e.g., Young et al., 2016). It should be noted that  $^{17}\text{O}$  analyses without the  $\tau$ -correction would result in a significant inaccuracy in  $\delta^{17}\text{O}_{\text{RAW}}$  and  $\Delta^{17}\text{O}_{\text{RAW}}$  values (1.5‰) because the secondary ion intensity rapidly increases at the beginning of each analysis (0.2%/s, Figure 2). The internal and external errors of  $\Delta^{17}\text{O}_{\text{RAW}}$  of UWC-3 were typically 0.2–0.3‰ (2SE) and 0.2–0.4‰ (2SD), respectively, which are consistent with statistical uncertainties.

A set of dolomite–ankerite and magnesite–siderite standards (Śliwiński et al., 2016, 2018) were analyzed in the same SIMS session to evaluate the SIMS instrumental biases. While the  $\delta^{17}\text{O}$  of these carbonate standards (including UWC-3 calcite) are not known, we assume the  $\Delta^{17}\text{O} = 0$  for these standards, which should be good for the SIMS analyses with precisions of  $\sim 0.2\%$ . The secondary  $^{16}\text{O}^-$  intensities were  $\sim 2 \times 10^9$  cps for dolomite and magnesite, similar to calcite, while they were higher for Fe-rich carbonates, such as siderite having an intensity of

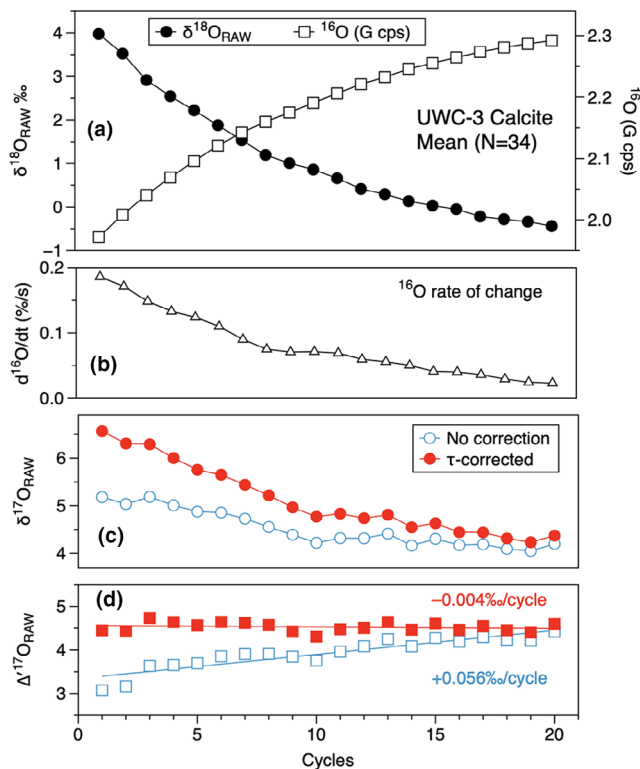


FIGURE 2. The  $\tau$ -correction (time constant correction) for  $^{17}\text{O}$  analyses using a  $10^{12}$  ohm feedback resistor. A total of 34 UWC-3 analyses were averaged. (a) Changes in  $^{18}\text{O}/^{16}\text{O}$  ratios ( $\delta^{18}\text{O}_{\text{RAW}}$ ) and  $^{16}\text{O}$  intensity (cps) with cycles. (b) Rate of change for  $^{16}\text{O}$  signal intensity (%/s). (c) Changes in  $^{17}\text{O}/^{16}\text{O}$  ratios ( $\delta^{17}\text{O}_{\text{RAW}}$ ) with cycles. Without  $\tau$ -correction,  $\delta^{17}\text{O}_{\text{RAW}}$  is lower by  $(d^{16}\text{O}/dt) \times \tau$  due to the slow response in  $10^{12}$  ohm feedback resistor. (d) Mass fractionation corrected  $\Delta^{17}\text{O}_{\text{RAW}}$  values with and without  $\tau$ -correction. Without  $\tau$ -correction, apparent mass-independent fractionation with the depth of analyses is observed.

$3 \times 10^9$  cps. The internal errors of  $\delta^{18}\text{O}_{\text{RAW}}$  and  $\delta^{17}\text{O}_{\text{RAW}}$  for these carbonate range 0.2–1.0‰ and 0.2–0.6‰, respectively, while external errors are typically 0.3–0.4‰, except for a few standards that are relatively heterogeneous (0.5–1.5‰ in 2SD for  $\delta^{18}\text{O}_{\text{RAW}}$ ). The instrumental biases of carbonate standards (bias) are expressed as relative biases (bias\*) against the UWC-3 calcite standard, as in Equations (2a and 2b).

$$\text{bias} = \left\{ \frac{(1 + \delta^{18}\text{O}_{\text{RAW}}/1000)}{(1 + \delta^{18}\text{O}/1000)} - 1 \right\} \times 1000 \quad (2a)$$

$$\text{bias}^* = \left\{ \frac{(1 + \text{bias}/1000)}{(1 + \text{bias}_{\text{UWC-3}}/1000)} - 1 \right\} \times 1000 \quad (2b)$$

All carbonate standards in this work showed a large negative bias from  $-24\text{‰}$  in UWMgs1 magnesite to

$-5\text{‰}$  in UWAnk6a ankerite, while those of UWC-3 calcite and UW6220 dolomite were  $-11\text{‰}$  and  $-16\text{‰}$ , respectively. In Figure 3, the instrumental biases of dolomite–ankerite and magnesite–siderite are shown relative to UW6220 dolomite ( $\text{bias}^*_{\text{UW6220}}$ ) and UWMgs1 magnesite ( $\text{bias}^*_{\text{UWMgs1}}$ ), respectively, fitted against the carbonate Fe# (molar  $\text{Fe}/[\text{Fe} + \text{Mg}]$ ) by the method described in Śliwiński et al. (2016, 2018). Fitted functions are shown in Table S4. They were in good agreement with previous studies (Śliwiński et al., 2016, 2018; Yokoyama et al., 2023). Because Ryugu carbonates contain more Mn than those of the SIMS standards with similar Fe#, we estimated SIMS biases of carbonates as functions of Fe# as well as  $(\text{Fe} + \text{Mn})\#$  (molar  $[\text{Fe} + \text{Mn}]/[\text{Fe} + \text{Mn} + \text{Mg}]$ ), which are also shown in Figure 3. The residuals of the fitted curves are within  $\pm 0.5\text{‰}$ , as shown in Figure 3c–f. We calculated the 2SD of the residuals and assigned them as the uncertainties of instrumental bias corrections that are 0.7‰ for dolomite and 0.4‰–0.5‰ for breunnerite.

The raw measured  $\Delta^{17}\text{O}_{\text{RAW}}$  of dolomite–ankerite and magnesite–siderite standards were indistinguishable from that of the UWC-3 calcite running standard ( $\leq 0.2\text{‰}$ ), except for slightly higher values in dolomite and magnesite standards near Mg-rich endmembers (Figure S2). Since Ryugu carbonates are relatively Fe-rich compared to pure dolomite and magnesite, the  $\Delta^{17}\text{O}$  values of Ryugu dolomite and breunnerite are determined as the difference from running standard UWC-3 calcite. Instrumental bias-corrected results ( $\delta^{18}\text{O}$  and  $\delta^{17}\text{O}$ ) are calculated using the following formula.

$$\delta^{18}\text{O} = \left\{ \frac{(1 + \delta^{18}\text{O}_{\text{RAW}}/1000) \times (1 + \text{bias}^*/1000) - 1}{1000} \right\} \quad (3a)$$

$$\delta^{17}\text{O} = \left\{ \frac{(1 + \delta^{18}\text{O}/1000)^\beta \times (1 + \Delta^{17}\text{O}/1000) - 1}{1000} \right\} \quad (3b)$$

The mass-independent fractionation factors of Ryugu carbonates are calculated using the linear formula  $\Delta^{17}\text{O} = \delta^{17}\text{O} - 0.52 \times \delta^{18}\text{O}$  according to Clayton et al. (1991) for the convenience of comparing our results to literature.

### Magnetite Analyses

The analytical conditions are modified from those of Huberty et al. (2010) for lower primary ion impact energy and those of Ushikubo et al. (2012) for oxygen 3-isotope analyses using a smaller (3–4  $\mu\text{m}$ ) spot beam. The primary  $\text{Cs}^+$  ion beam was accelerated by +3 kV at the Cs ion

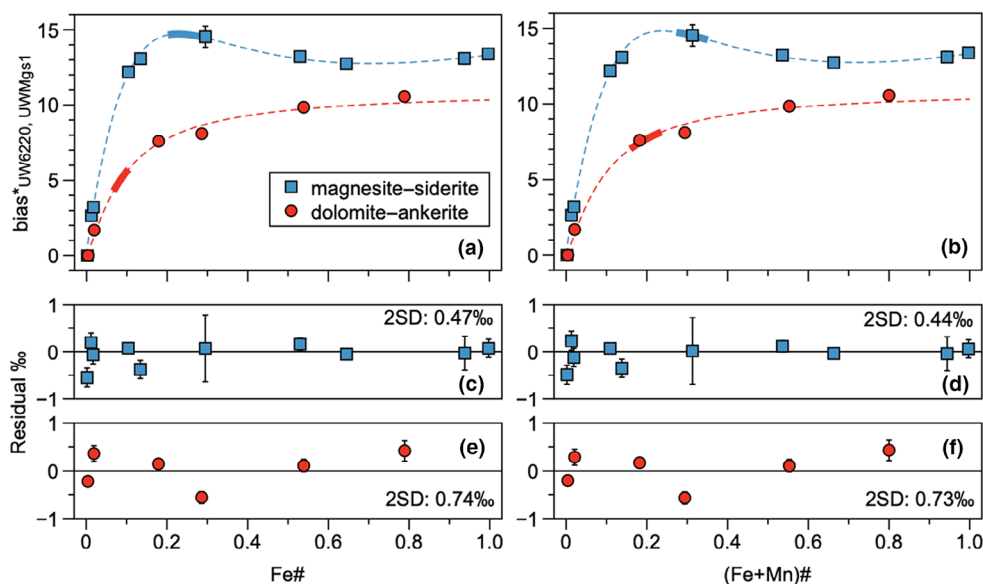


FIGURE 3. Instrumental bias correction of carbonates using two correction schemes using Fe# (a, c, e) and (Fe + Mn)# (b, d, f). (a, b) Instrumental biases in  $\delta^{18}\text{O}$  for magnesite–siderite and dolomite–ankerite that are fitted using Hill functions. The ranges of biases for carbonates in Ryugu are shown as thick curves. (c, d) Residual from fitted functions for magnesite–siderite. (e, f) Residual from fitted functions for dolomite–ankerite. Data are shown in Table S4.

source and focused to sample surface (at  $-10\text{ kV}$ ), resulting in an impact energy of  $13\text{ keV}$ . The primary beam was focused to  $3\text{ }\mu\text{m}$  with  $14\text{ pA}$  intensity and rastered over  $2\text{ }\mu\text{m}$  squares, which resulted in  $3\times 4\text{ }\mu\text{m}$  SIMS pits after 10 min of analysis. The  $^{16}\text{O}^-$  intensity was typically  $1.7\times 10^7$  cps for magnetite. Other conditions were similar to those of carbonate analyses, except for the configuration of detectors. Due to the lower secondary ion intensities of minor oxygen isotopes  $^{17}\text{O}^-$  ( $\sim 6\times 10^3$  cps) and  $^{18}\text{O}^-$  ( $3\times 10^4$  cps), they were detected by using EM on the axial detector and MC array, respectively. The  $^{16}\text{O}^-$  signals were detected by using FC on the MC array with a  $10^{11}$  ohm feedback resistor. A single analysis consisted of presputtering (60 s), beam centering, signal acquisition (400 s; 20 s  $\times$  20 cycles), EM gain adjustment, and  $^{16}\text{O}^1\text{H}^-$  monitoring at the end of each analysis. The internal errors and external reproducibility of a single grain of magnetite standard 5830 (Huberty et al., 2010) were 0.7–0.9‰ in  $\delta^{18}\text{O}$  and 1.5‰ in  $\delta^{17}\text{O}$  and  $\Delta^{17}\text{O}$ . The effect of crystal orientation was evaluated by using 30 randomly oriented grains of magnetite standard 5830 in the same session. The external reproducibility of  $\delta^{18}\text{O}_{\text{RAW}}$  was 1.0‰ (2SD), similar to the uncertainty of a single grain (Table S3, Figure S3), which was propagated to the final uncertainty of the unknown magnetite analyses. The external reproducibility of  $\Delta^{17}\text{O}_{\text{RAW}}$  of the same standard was 1.3‰ ( $n=42$ , Figure S3). The correction of  $^{16}\text{O}^1\text{H}^-$  to  $\delta^{17}\text{O}$  was insignificant for both standard and Ryugu samples ( $\leq 0.3\text{‰}$ ).

### Targeting Minerals in Ryugu

We took high-resolution reflected microscope images of each section (Data repository) and overlaid an x-ray elemental map by using the QGIS program with WiscSIMS plugins (Batchelor et al., 2022; Linzmeier et al., 2018). The high optical resolution ( $1.3\text{ }\mu\text{m}$ ) of the SIMS microscope with UV light illumination and Badgersscope© Camera viewing software (Kita et al., 2015) allowed us to aim at individual minerals precisely within  $2\text{ }\mu\text{m}$ . After the SIMS sessions, SIMS pits were inspected by using a Hitachi S-3400 SEM at the University of Wisconsin–Madison.

## RESULTS

### Magnetite

Magnetite grains analyzed in this study are relatively coarse-grained ( $\geq 5\text{ }\mu\text{m}$ ) with irregular, equant, or spherulitic textures. A total of 27 analyses of magnetite were obtained, 17 from A0058-C1002 and 10 from C0002-C1001. SEM observations of the pits after SIMS analyses show that all SIMS spots were within the targeted magnetite grains (Data repository), thus none of the analyses were rejected. There are two types of pit textures: smooth and porous, which often correspond to magnetite with defined crystal faces and fibrous grains, respectively (Figure 4). The smooth texture is identical to those of the magnetite standard. Examples of porous textures are Figure 4b,c, where the bottom of SIMS craters show

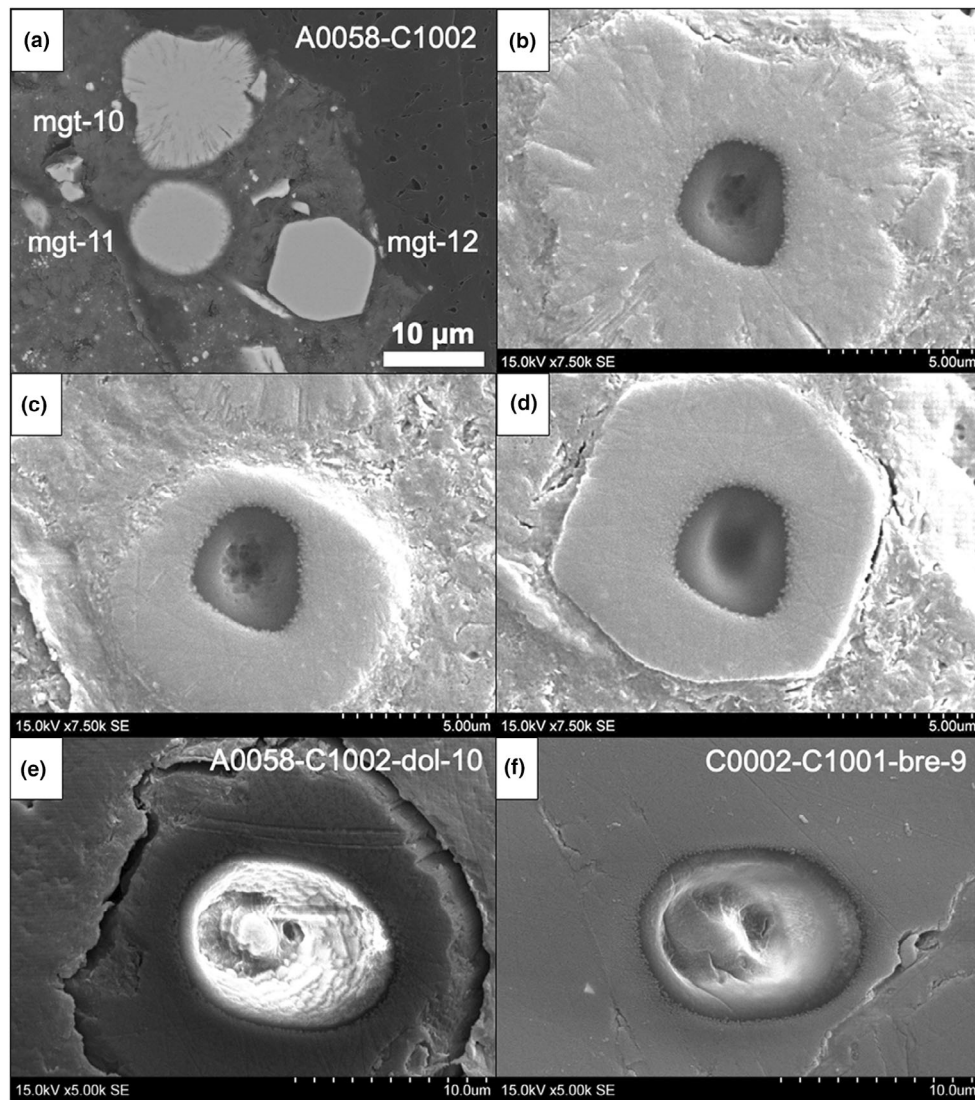


FIGURE 4. Magnetite and carbonate SIMS pits. (a) BSE image of three magnetite grains (mgt-10, -11, -12) in A0058-C1002. (b–d) Secondary electron (SE) images of SIMS pits from the magnetite grains in (a), showing porous (b, c) and smooth (d) pit textures. (e) SE image of dolomite. (f) SE image of breunnerite.

multiple  $\mu\text{m}$ -sized pits. Results of analyses are shown in Table 1, Table S3, and Figure 5 and compared to those reported by Nakamura et al. (2022), Yokoyama et al. (2023), and McCain et al. (2023) using 20 keV impact energy, as well as magnetite separate in CI chondrite (Rowe et al., 1994) and magnetite analyses of Ivuna reported by Yokoyama et al. (2023). Overall, our data are consistent with those reported earlier and plot slightly above the PCM (Primitive Chondrule Mineral) line (Ushikubo et al., 2012). New data show two groups of magnetite analyses according to the range of  $\delta^{18}\text{O}$  values, from  $-4\text{‰}$  to  $+1\text{‰}$  and from  $+3\text{‰}$  to  $+7\text{‰}$ , which correspond to magnetite grains with smooth and porous pit textures, respectively. The  $\Delta^{17}\text{O}$  values of the lower  $\delta^{18}\text{O}$  group vary from  $0\text{‰}$  to  $+2\text{‰}$ ,

while the higher  $\delta^{18}\text{O}$  group shows consistently higher  $\Delta^{17}\text{O}$  values ( $2.1 \pm 0.5\text{‰}$ , 2SD,  $n = 11$ ). The  $^{16}\text{O}^1\text{H}^- / ^{16}\text{O}^-$  signal ratios (not background corrected) of magnetite with porous SIMS pits are systematically higher than those of smooth pits in each Ryugu section.

Analyses of magnetite in the pyrrhotite–magnetite–dolomite assemblage in A0058-C1002 (Figure S4; spots 4–5, 13–16, 18) show a narrow range of oxygen isotope ratios with the mean values of  $\delta^{18}\text{O} = -2.6 \pm 1.2\text{‰}$ ,  $\delta^{17}\text{O} = -1.0 \pm 1.1\text{‰}$ ,  $\Delta^{17}\text{O} = 0.3 \pm 0.6\text{‰}$  (2SD,  $n = 7$ ). These data agree with the mean of four magnetite analyses that were used for magnetite–dolomite oxygen isotope thermometry in Yokoyama et al. (2023). There are three analyses of magnetite from two coarser-grained



TABLE 1. Oxygen isotope analyses of magnetite (mgt) in Ryugu.

Section and spot	SIMS pit texture	$\delta^{18}\text{O}$ (‰)	Unc.	$\delta^{17}\text{O}$ (‰)	Unc.	$\Delta^{17}\text{O}$ (‰)	Unc.	$^{16}\text{O}^{1}\text{H}/^{16}\text{O}^{\text{a}}$
<i>A0058-C1002 pyr-dol-mgt<sup>b</sup></i>								
mgt-4	Smooth	-2.6	1.0	-1.1	1.1	0.2	1.2	0.0026
mgt-5	Smooth	-2.6	1.0	-1.1	1.1	0.3	1.2	0.0029
mgt-13	Smooth	-2.7	1.0	-1.4	1.1	0.0	1.2	0.0028
mgt-14	Smooth	-1.5	1.0	-0.4	1.1	0.4	1.2	0.0027
mgt-15	Smooth	-3.5	1.0	-2.0	1.4	-0.1	1.3	0.0024
mgt-16	Smooth	-2.6	1.0	-0.6	1.4	0.7	1.3	0.0030
mgt-18	Smooth	-2.7	1.0	-0.8	1.1	0.6	1.2	0.0027
Mean and 2SD		-2.6	1.2	-1.0	1.1	0.3	0.6	0.0027
<i>A0058-C1002 others</i>								
mgt-1	Smooth	-1.0	1.0	0.2	1.1	0.8	1.2	0.0027
mgt-2	Smooth	-3.0	1.0	-1.0	1.4	0.5	1.3	0.0025
mgt-6	Smooth	-3.0	1.0	-1.8	1.1	-0.3	1.2	0.0025
mgt-7	Porous	3.3	1.0	3.3	1.4	1.6	1.3	0.0045
mgt-8	Smooth	-1.2	1.0	-0.3	1.4	0.3	1.3	0.0025
mgt-10	Porous	6.5	1.0	5.5	1.4	2.1	1.3	0.0067
mgt-11	Porous	4.9	1.0	4.8	1.4	2.3	1.3	0.0070
mgt-12	Smooth	-2.4	1.0	0.4	1.4	1.6	1.3	0.0026
mgt-17	Porous	6.5	1.0	5.3	1.1	1.9	1.2	0.0038
mgt-19	Porous	7.2	1.0	5.9	1.4	2.2	1.3	0.0038
<i>C0002-C1001</i>								
mgt-5	Smooth	-3.5	1.0	0.3	1.9	2.1	1.9	0.0052
mgt-8	Porous	4.3	1.0	4.4	1.9	2.1	1.9	0.0102
mgt-9	Porous	4.1	1.0	4.5	1.9	2.4	1.9	0.0083
mgt-11	Porous	5.6	1.0	5.1	1.9	2.2	1.9	0.0080
mgt-14	Porous	5.3	1.0	4.4	1.9	1.7	1.9	0.0070
mgt-15	Smooth	-3.7	1.0	0.0	1.9	2.0	1.9	0.0061
mgt-16	Smooth	0.6	1.0	2.3	1.9	2.0	1.9	0.0072
mgt-17	Smooth	-3.4	1.0	-0.3	1.9	1.4	1.9	0.0054
mgt-18	Porous	3.4	1.0	3.8	1.9	2.0	1.9	0.0074
mgt-19	Porous	5.3	1.0	5.1	1.9	2.4	1.9	0.0067
Porous pits mean and 2SD		5.1	2.6	4.7	1.5	2.1	0.5	0.0067

Note: Uncertainties quoted with the data are at the 95% confidence level and include those from instrumental bias corrections.

<sup>a</sup>Values are not corrected for chamber background.

<sup>b</sup>Pyrrhotite–dolomite–magnetite assemblage shown in Figure S4.

framboids: spots 15 and 16 in C0002-C1001 (smooth pits) and spot 7 in A0058-C1002 (porous pit). They show a variable  $\delta^{18}\text{O}$  but consistently show a higher  $\Delta^{17}\text{O} \sim 2\text{‰}$ .

### Dolomite and Breunnerite

A total of 29 analyses of carbonate were obtained: 18 dolomite (9 from each section) and 11 breunnerite in C0002-C1001. Three dolomite and two breunnerite analyses show a significant decrease in the secondary  $^{16}\text{O}^-$  intensity at the middle of the analyses. The SEM inspection of the SIMS pits (Figure 4) revealed that these analyses overlapped with grain boundaries and cracks, so that these data were rejected. Results are shown in Table 2, Table S5, and Figures 6 and 7 using the two different instrumental bias correction schemes (Figure 3). They plot on or slightly above the terrestrial mass fractionation line (TFL). Some of

dolomite analyses with relatively large uncertainties in Fe# ( $>0.02$ ) are quoted with uncertainties larger than 1‰ and 0.5‰ in  $\delta^{18}\text{O}$  and  $\delta^{17}\text{O}$ , respectively, due to larger uncertainties in the instrumental bias estimates. Dolomite analyses corrected for Fe# (Figure 2a) are consistent with those determined previously by Yokoyama et al. (2023) and are within a range reported by McCain et al. (2023), and dolomite data from Ivuna by Yokoyama et al. (2023). Data corrected for (Fe + Mn)# show lower  $\delta^{18}\text{O}$  by 2–3‰ (Figure 2b) than those corrected for Fe#. Breunnerite contains more Fe than Mn, so that bias-corrected data in Figures 6a,b and 7a,b are very similar. Most breunnerite data plot at lower  $\delta^{18}\text{O}$  ( $\sim 21\text{‰}$ ) compared to dolomite. The  $\delta^{18}\text{O}$  from three breunnerite analyses are  $\sim 5\text{‰}$  higher than others and overlap within the range of dolomite. They are from two breunnerite grains with distinct chemical compositions, either a Fe-rich (spots 1 and 2; 33 mole%

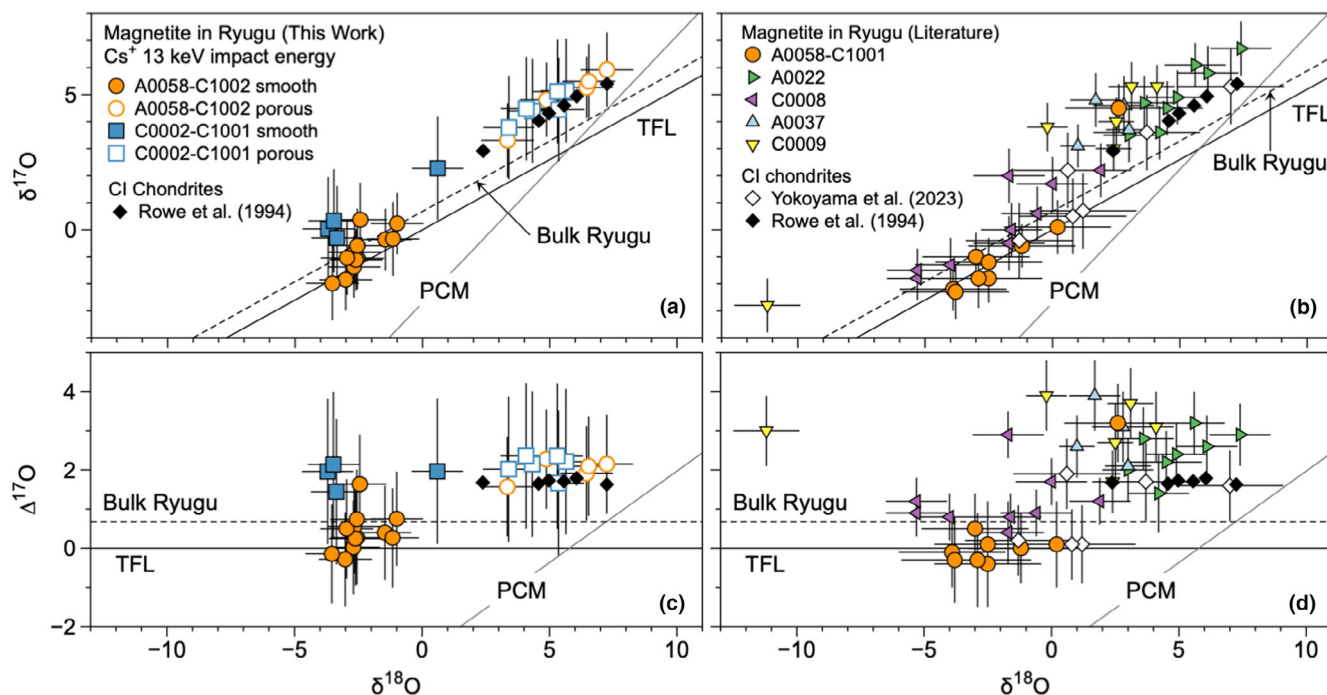


FIGURE 5. Magnetite oxygen isotope analyses in Ryugu. (a) Oxygen three-isotope plot for magnetite in A0058-C1002 and C0002-C1001 (this work). Filled and open symbols are for smooth and porous SIMS pits, respectively. (b) Oxygen three-isotope plot for magnetite in Ryugu from Yokoyama et al. (2023; A0058), Nakamura et al. (2022; A0022, C0008), and McCain et al. (2023; A0037, C0009). Magnetite separates from CI chondrite Alais, Ivuna, and Orgueil (Rowe et al., 1994) and SIMS magnetite data from Ivuna (Yokoyama et al., 2023) are shown for comparison. (c, d) The plot showing  $\Delta^{17}\text{O}$  versus  $\delta^{18}\text{O}$  for the same samples in a and b, respectively. PCM line and TFL (terrestrial fractionation line) are shown as reference. The dashed lines indicate the slope 0.52 line that passes the bulk Ryugu oxygen isotope ratios.

$\text{FeCO}_3$ ) or a Mn-rich (spot 11; 11 mole%  $\text{MnCO}_3$ ) compared to remaining breunnerite grains (25 mole%  $\text{FeCO}_3$  and 3 mole%  $\text{MnCO}_3$ ). Nakamura et al. (2022) reported substantially higher  $\delta^{18}\text{O}$  in dolomite (30–40‰) compared to this work, Yokoyama et al. (2023), and McCain et al. (2023). Their analyses were corrected by a single dolomite standard, so that the instrumental correction might not be adequately done. They are not shown in Figures 6 and 7. Figures 6 and 7 include Orgueil and Ivuna dolomite analyses by Piralla et al. (2020) that show a similar range to those of Ryugu dolomite using Fe# correction, though details of the instrumental bias correction in Piralla et al. (2020) are not known.

The  $\Delta^{17}\text{O}$  values of dolomite and breunnerite data are within a narrow range from 0‰ to 0.8‰. There is a small systematic difference between A0058-C1002 and C0002-C1001 with the mean values of  $0.17 \pm 0.22\text{‰}$  (2SD,  $n=7$ ) and  $0.47 \pm 0.33\text{‰}$  (2SD,  $n=17$ ), respectively. The  $\Delta^{17}\text{O}$  values between dolomite and breunnerite in C0002-C1001 are indistinguishable. These data are within the range reported by Yokoyama et al. (2023) and McCain et al. (2023). We note that dolomite analyses by Nakamura et al. (2022) show systematically higher  $\Delta^{17}\text{O}$  ( $1.4 \pm 0.9\text{‰}$ , 2SD,  $n=29$ ).

The dolomite grains in the pyrrhotite–magnetite–dolomite assemblage in A0058-C1002 (Figure S4; spots 4, 7, 9–10) show indistinguishable oxygen isotope ratios with the mean values of  $\delta^{18}\text{O} = 28.3 \pm 1.9\text{‰}$  and  $\delta^{17}\text{O} = 14.9 \pm 0.9\text{‰}$  using the Fe# correction,  $\delta^{18}\text{O} = 25.1 \pm 1.9\text{‰}$  and  $\delta^{17}\text{O} = 13.2 \pm 0.9\text{‰}$  using the (Fe + Mn)# correction, and  $\Delta^{17}\text{O} = 0.18 \pm 0.29\text{‰}$  (2SD,  $n=4$ ). Fe# corrected data agree with the dolomite analyses that were used for magnetite–dolomite oxygen isotope thermometry in Yokoyama et al. (2023).

## DISCUSSION

### Morphology of Magnetite and Oxygen Isotope Ratios

Magnetite in Ryugu and CI chondrites occur in multiple morphologies: framboidal, spherules, plaquettes, or equant shapes with a variety of sizes from nm to  $\geq 10\ \mu\text{m}$  (e.g., Alfing et al., 2019; Nakamura et al., 2023; Tsuchiyama et al., 2022). Dobrică et al. (2023) examined the microstructure of spherulitic magnetite in Ryugu by using TEM and found radiating fibers, nanometric pores, and pervasive dislocations, which are indicative of disequilibrium crystallization from aqueous fluid. One key

TABLE 2. Oxygen isotope analyses of dolomite (dol) and breunnerite (bre) in Ryugu.

Sections, spot	Fe#	unc	$\delta^{18}\text{O}$ ‰	Unc.	$\delta^{17}\text{O}$ ‰	Unc.	(Fe + Mn)#	unc	$\delta^{18}\text{O}$ ‰	Unc.	$\delta^{17}\text{O}$ ‰	Unc.	$\Delta^{17}\text{O}$ ‰	Unc.
<i>A0058-C1002 prr-dol-mgt</i>														
dol-4	0.071	0.014	27.0	1.0	14.3	0.6	0.195	0.039	23.7	+1.0/−0.9	12.6	0.5	0.29	0.23
dol-7	0.068	0.027	29.1	+1.7/−1.3	15.4	0.9	0.192	0.014	25.8	0.8	13.7	0.4	0.26	0.20
dol-9	0.079	0.016	28.4	1.0	15.0	0.6	0.201	0.040	25.5	+1.0/−0.9	13.4	0.5	0.19	0.24
dol-10	0.067	0.007	28.6	0.8	14.8	0.5	0.177	0.040	25.4	+1.1/−0.9	13.2	0.6	−0.03	0.26
Mean and 2SD			28.3	1.9	14.9	0.9		25.1		1.9	13.2	0.9	0.18	0.29
<i>A0058-C1002 other</i>														
dol-5	0.079	0.016	27.6	1.0	14.5	0.6	0.202	0.040	24.6	+1.0/−0.9	12.9	0.5	0.14	0.24
dol-6	0.081	0.013	27.7	0.9	14.7	0.5	0.190	0.021	25.0	0.8	13.3	0.5	0.24	0.29
dol-8	0.080	0.037	28.0	+2.0/−1.5	14.7	1.1	0.207	0.040	25.0	+1.0/−0.9	13.1	0.5	0.10	0.29
<i>A0058-C1002 mean and 2SD</i>														
<i>C0002-C1001 major breunnerite</i>														
bre-4	0.255	0.006	20.7	0.5	11.1	0.3	0.278	0.006	20.7	0.5	11.1	0.3	0.36	0.26
bre-5	0.251	0.003	21.2	0.5	11.4	0.3	0.273	0.004	21.2	0.5	11.4	0.3	0.39	0.24
bre-7	0.265	0.004	21.1	0.5	11.2	0.3	0.289	0.004	21.1	0.5	11.2	0.3	0.23	0.21
bre-9	0.257	0.003	21.4	0.5	11.5	0.3	0.279	0.003	21.4	0.5	11.5	0.3	0.35	0.24
bre-8	0.257	0.003	21.8	0.5	11.8	0.3	0.279	0.003	21.8	0.5	11.8	0.3	0.46	0.27
bre-13	0.263	0.008	21.4	0.5	11.5	0.3	0.285	0.009	21.3	0.5	11.5	0.3	0.42	0.35
Mean and 2SD			21.3	0.7	11.4	0.5		21.2		0.7	11.4	0.5	0.37	0.16
<i>C0002-C1001 other</i>														
bre-1 (Fe-rich)	0.337	0.004	26.2	0.5	14.4	0.3	0.351	0.005	26.1	0.5	14.4	0.3	0.79	0.23
bre-2 (Fe-rich)	0.337	0.004	26.5	0.5	14.2	0.3	0.351	0.005	26.4	0.5	14.2	0.3	0.44	0.22
bre-11 (Mn-rich)	0.202	0.015	26.9	0.5	14.5	0.3	0.289	0.018	26.9	0.5	14.5	0.3	0.46	0.24
dol-9	0.082	0.010	28.6	+0.9/−0.8	15.3	0.5	0.215	0.012	25.6	0.8	13.7	0.4	0.43	0.24
dol-3	0.104	0.028	25.3	+1.3/−1.1	13.4	0.7	0.236	0.033	22.9	0.8	12.1	0.5	0.24	0.26
dol-8	0.085	0.019	28.7	+1.1/−1.0	15.5	0.6	0.176	0.024	26.4	+0.9/−0.8	14.3	0.5	0.58	0.27
dol-2	0.075	0.003	28.6	0.8	15.2	0.4	0.178	0.004	25.8	0.7	13.8	0.4	0.38	0.24
dol-5	0.092	0.013	26.9	0.9	14.5	0.5	0.172	0.016	24.9	0.8	13.5	0.4	0.56	0.22
dol-10	0.089	0.018	26.9	1.1	14.8	0.6	0.186	0.022	24.6	0.8	13.6	0.5	0.80	0.23
dol-10p	0.076	0.023	29.5	+1.3/−1.1	15.7	0.7	0.175	0.029	26.9	0.9	14.3	0.5	0.37	0.26
dol-11	0.092	0.020	27.2	+1.1/−1.0	14.8	0.6	0.198	0.025	24.8	0.8	13.6	0.5	0.69	0.23
<i>C0002-C1001 mean and 2SD</i>														

Note: Uncertainties quoted with the data are at the 95% confidence level and include those from instrumental bias corrections.

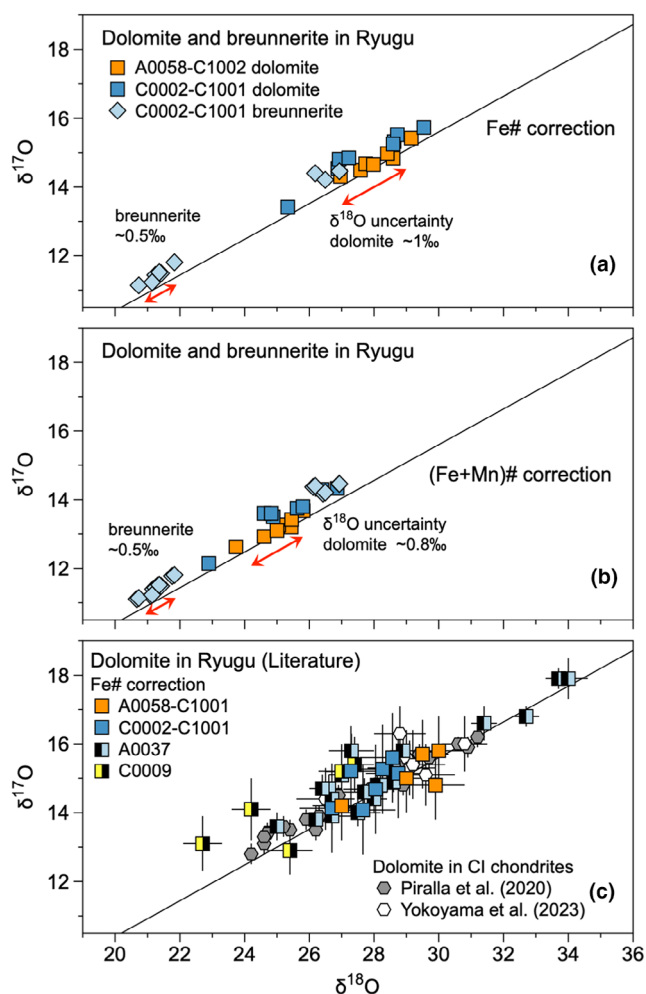


FIGURE 6. Carbonate–oxygen isotope analyses in Ryugu. (a) Data from A0058-C1002 and C0002-C1001 from this work with the bias correction using Fe#. (b) The same data set with the bias correction using (Fe + Mn)#. (c) Literature data for Ryugu dolomite (Fujiya et al., 2023; McCain et al., 2023; Yokoyama et al., 2023) and dolomite analyses in CI chondrites (Piralla et al., 2020; Yokoyama et al., 2023).

observation from Ryugu magnetite analyses in this study is the correlation between oxygen 3-isotope ratios and the SIMS pit morphologies. High-resolution SEM images of magnetite with porous SIMS pits show that they are spherulitic magnetite, some of which show radiating fibers and/or a complex microstructure at the outer edge (Figure 4), similar to those described by Dobrică et al. (2023). The porous SIMS pit morphologies in these magnetite spherules are likely caused by heterogeneous sputtering of the samples, which contain numerous nanometer-sized pores. In contrast, smooth SIMS pit morphologies were observed from magnetite with well-defined crystal faces, which are similar to magnetite with equant morphologies (Dobrică et al., 2023). Systematically higher  $^{16}\text{O}^1\text{H}^-$  signals in spherulitic magnetite are

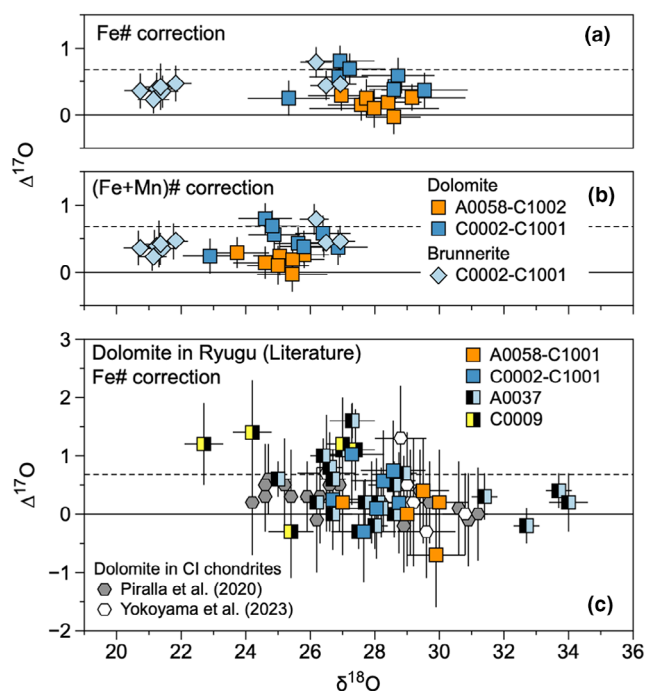


FIGURE 7.  $\Delta^{17}\text{O}$  versus  $\delta^{18}\text{O}$  for carbonate in Ryugu. a, b, and c correspond to the same data set and bias correction schemes in Figure 6a–c, respectively.

consistent with the NanoSIMS analyses of H concentrations that are systematically higher in spherulitic magnetite (Aléon et al., 2024). Due to the correlation between H and Si signals among fibrous magnetite analyses, Aléon et al. (2024) suggested that the nano-scale phyllosilicates were trapped in the magnetite, which are related to Si-rich amorphous materials observed by Dobrică et al. (2023) by TEM.

From x-ray nanotomography of magnetite in Ryugu, Tsuchiyama et al. (2022) suggested that the morphologies of magnetite changed with the crystallization sequence in the order of spherulitic, plaquette/framboidal, and equant/elongated. Our results suggest that the early formed spherulitic magnetite (with porous SIMS pits) recorded systematically higher  $\delta^{18}\text{O}$  than those of later formed equant/elongated (with smooth SIMS pits) magnetite. Moreover, the early formed magnetite grains consistently show higher  $\Delta^{17}\text{O} \sim +2\text{‰}$ , while those of later formed magnetite grains are variable from 0‰ to 2‰. These data indicate that the aqueous fluid on the Ryugu parent asteroid started from  $\Delta^{17}\text{O}$  higher than  $\sim +2\text{‰}$ .

### Oxygen Isotope Thermometry

The oxygen isotope fractionation factors of magnetite and carbonate against water decrease with the increase of temperatures from 0 to 100°C, where changes are greater for carbonate than magnetite, from  $\delta^{18}\text{O}$  of  $\sim 0\text{‰}$  to  $-6\text{‰}$

or  $-7\%$  for magnetite and from  $40\%$  to  $20\%$  for carbonates (Hayles et al., 2018; Zheng, 1991, 1999; Table S6). There are only small differences ( $\leq 2\%$ ) among carbonate minerals (calcite, dolomite, and breunnerite). Oxygen thermometry by using a pair of magnetite and a carbonate is useful in the estimation of the temperature of the aqueous fluid from which they grew because of the strong temperature dependency of isotope fractionation between the two minerals (e.g., Yokoyama et al., 2023).

Nakamura et al. (2023) provided several mineralogical constraints on the temperatures of aqueous alteration in Ryugu parent body. The temperature of alteration was likely lower than  $100^\circ\text{C}$  due to the low abundance of Mg-chlorite. The lattice spacing and the chemical compositions of pentlandite indicate the equilibrium temperatures of  $20 \pm 29.5^\circ\text{C}$ . Yokoyama et al. (2023) estimated the temperature of aqueous fluid by applying oxygen isotope thermometry according to the calculated fractionation factors by Zheng (1991, 1999). They estimated the temperature of  $37 \pm 10^\circ\text{C}$  from a set of magnetite and dolomite analyses in the section A0058-C1001 with  $\delta^{18}\text{O}$  values of  $-3.0 \pm 1.1\%$  and  $29.9 \pm 0.9\%$ , respectively. This temperature range is consistent with the mineralogical constraints as discussed by Nakamura et al. (2023).

In order to apply thermometry, these two minerals should be on the same mass-dependent fractionation line; they do show indistinguishable  $\Delta^{17}\text{O}$  of  $-0.1 \pm 0.4\%$  for magnetite and  $-0.7 \pm 0.9\%$  for dolomite. In this work, we confirmed that magnetite and dolomite in the coarse-grained pyrrhotite–dolomite–magnetite assemblages of A0058-C1002 are indistinguishable in  $\Delta^{17}\text{O}$  values, with the mean of  $0.30 \pm 0.60\%$  (2SD,  $n=7$ ) and  $0.18 \pm 0.29\%$  (2SD,  $n=4$ ), respectively. The mean of the  $\delta^{18}\text{O}$  in these magnetite and dolomite in this work are  $-2.6 \pm 1.1\%$  (2SE) for magnetite and  $28.3 \pm 0.8\%$  and  $25.1 \pm 0.8\%$  by using Fe# and (Fe + Mn)# corrections, respectively. Using these values, we estimated equilibrium temperatures of  $51 \pm 11^\circ\text{C}$  and  $78 \pm 14^\circ\text{C}$  for dolomite with Fe# and (Fe + Mn)# corrections, respectively (Table S6). The estimated temperature using Fe# correction agrees with that of Yokoyama et al. (2023) within the uncertainties. The dolomite standards used for the instrumental bias correction do not contain as much Mn as those in Ryugu, so that effect of Mn on the SIMS instrumental bias is unknown. Accurate estimates of the equilibrium temperatures require the development of Mn-bearing dolomite standards.

McCain et al. (2023) further estimated the temperatures of calcite–magnetite pairs with higher  $\Delta^{17}\text{O}$  (using fractionation factors of Hayles et al., 2018) in C0009 to be  $0\text{--}20^\circ\text{C}$ . They consider this mineral pair to have formed in the early stage of aqueous alteration because of the higher  $\Delta^{17}\text{O}$ , which represents a less-equilibrated fluid composition. Calcite with high  $\delta^{18}\text{O}$  and  $\Delta^{17}\text{O}$ , similar to that in McCain et al. (2023), were also observed by Fujiya

et al. (2023) from less-altered areas in C0002-C1001. We note that spherulitic magnetite in this study shows similar  $\delta^{18}\text{O}$  and  $\Delta^{17}\text{O}$  to magnetite grains analyzed by McCain et al. (2023), as shown in Figure 5. The detailed textures of magnetite grains in C0009 and their SIMS pit morphologies are not reported in McCain et al. (2023) and Yamaguchi et al. (2023). Therefore, it is not clear if they are spherulitic or fibrous magnetite that might have formed under nonequilibrium conditions (Dobrică et al., 2023). If they were spherulitic magnetite, oxygen isotopes might not be in equilibrium with the fluid, and the estimated temperature of  $0\text{--}20^\circ\text{C}$  should be treated with caution.

All magnetite analyses in C0002-C1001 show significantly higher  $\Delta^{17}\text{O}$  ( $\sim 2\%$ ) than those in dolomite and breunnerite ( $\sim 0.5\%$ ), indicating that oxygen isotope thermometry cannot be applied for magnetite–dolomite or magnetite–breunnerite in C0002. As an exceptional case, Nagashima et al. (2022) reported a pair of magnetite and dolomite in C0002 that are located within  $100\ \mu\text{m}$  of each other and have an indistinguishable  $\Delta^{17}\text{O}$  of  $+0.6\%$ . The estimated equilibrium temperature for this mineral pair is  $92 \pm 21^\circ\text{C}$  (Nagashima et al., 2022).

The equilibrium isotope fractionation between breunnerite and dolomite are small at the temperature range of  $0\text{--}100^\circ\text{C}$  ( $\Delta^{18}\text{O}_{\text{dol-bre}} = 0.5\text{--}1.0\%$ ; Zheng, 1999). Three breunnerite data overlap with dolomite data in Figures 6 and 7, suggesting that they might have formed under the equilibrium with dolomite. These breunnerite data are from those with Fe-rich or Mn-rich breunnerite. We did not find any dolomite associated with these breunnerite grains to test the equilibrium relationship. The majority of breunnerite grains, including large  $\geq 100\ \mu\text{m}$  crystals, show  $\delta^{18}\text{O}$  values significantly lower than dolomite by  $5\%$  or  $7\%$ . Such a large difference could be caused by the temperature difference of  $20\text{--}30^\circ\text{C}$  (higher for breunnerite) if the oxygen isotope ratios of the aqueous fluid were the same.

### Oxygen Isotope Evolution of the Aqueous Fluid

Here we compare oxygen isotope systematics among magnetite and carbonate in Ryugu to the chemical equilibrium model of the aqueous alteration of Ryugu parent body presented by Nakamura et al. (2023). The model involves equilibrium among minerals, solution, and gas phases at the variable water-to-rock ratios (W/R; in mass) at temperatures of  $0\text{--}40^\circ\text{C}$  and generally explains the diverse mineral assemblages observed in Ryugu samples. Magnetite and calcite would form in less-altered conditions (W/R: 0.1–0.2), which is similar to less-altered lithologies found in C0002 containing anhydrous silicates such as olivine, pyroxene, CAIs, and chondrules (e.g., Kawasaki et al., 2022; Nakashima et al., 2023). In contrast, magnetite and dolomite would form in more-altered conditions (W/R:

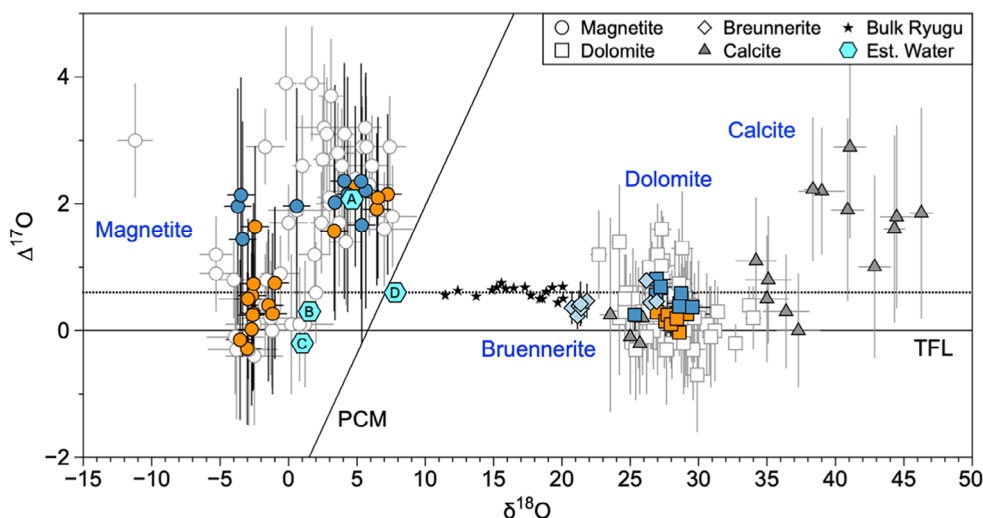


FIGURE 8. Magnetite and carbonate isotope analyses in Ryugu from this work and literature (Fujiya et al., 2023; McCain et al., 2023; Nakamura et al., 2022; Yokoyama et al., 2023) as well as those of CI chondrites (Piralla et al., 2020; Rowe et al., 1994; Yokoyama et al., 2023). Dolomite data from this work are those with Fe# corrections. Bulk analyses are also shown for comparison (Greenwood et al., 2022; Nakamura et al., 2022; Yokoyama et al., 2023). Oxygen isotope ratios of water are estimated from magnetite analyses and shown as A–D (see text for explanation).

0.2–0.9), similar to major extensively altered lithologies with pyrrhotite–magnetite–dolomite assemblages found in A0058 (e.g., Yokoyama et al., 2023). The model also indicates that the formation of breunnerite (magnesite in the model) would require higher W/R ratios ( $\geq 0.7$ ). Nakamura et al. (2023) further argued that the Ryugu parent asteroid accreted  $\sim 2$  Ma after CAIs when  $^{26}\text{Al}$  abundance was sufficient as an internal heat source. Less-altered and more-altered lithologies were produced at the different depth where temperature and W/R were relatively lower near the asteroid surface than interior.

In Figure 8, the oxygen isotope ratios of magnetite and carbonates from Ryugu samples are shown as  $\Delta^{17}\text{O}$  versus  $\delta^{18}\text{O}$  from this study and literature. We find  $\Delta^{17}\text{O}$  of carbonate changes in the order of calcite ( $0\text{--}2\text{‰}$ )  $\geq$  dolomite  $\sim$  breunnerite ( $0\text{--}0.8\text{‰}$ ) in the same order of increasing W/R in the chemical equilibrium model. It is likely that spherulitic magnetite in both A0058-C1002 and C0002-C1001 with high  $\Delta^{17}\text{O}$  ( $\sim 2\text{‰}$ ) formed under less-altered and lower W/R conditions, while euhedral magnetite in A0058 with low  $\Delta^{17}\text{O}$  ( $\sim 0\text{‰}$ ) formed in more-altered and higher W/R conditions. Under the less-altered conditions, oxygen isotopes might not be fully exchanged between anhydrous silicates and aqueous fluid. The initial water accreted to the Ryugu parent body would have  $\Delta^{17}\text{O}$  significantly higher than  $+2\text{‰}$ , and aqueous fluid at the early stage was produced by the mixing between water ( $\Delta^{17}\text{O} > +2\text{‰}$ ) and anhydrous solids ( $\Delta^{17}\text{O}$  lower than bulk  $< 0.7\text{‰}$ ). Under more-altered conditions, oxygen isotopes might have

extensively exchanged between aqueous fluid and solid phases, resulting in  $\Delta^{17}\text{O}$  similar to that of bulk Ryugu samples.

Here, we apply a simple mass balance model to estimate the  $\Delta^{17}\text{O}$  value of aqueous fluid for the range of W/R from 0.2 to 0.9 that would produce the dolomite in more-altered lithology abundant in Ryugu samples. Because we do not know the initial  $\Delta^{17}\text{O}$  of water and anhydrous solids that accreted to the parent body, they were given as parameters in the model from  $2\text{‰}$  to  $5\text{‰}$  for water and from  $-5\text{‰}$  to  $0\text{‰}$  for solids, respectively (Figure 9, Table S7). The model indicates that the aqueous fluid with a narrow range of  $\Delta^{17}\text{O}$  from  $0.0\text{‰}$  to  $0.8\text{‰}$  requires a limited range of W/R if  $\Delta^{17}\text{O}$  of water and anhydrous solids were  $> 2\text{‰}$  and  $\leq -2\text{‰}$ , respectively. Rare mafic silicates observed in the less-altered areas in Ryugu as well as those in other CI chondrites typically show  $\Delta^{17}\text{O}$  from  $-5\text{‰}$  to  $0\text{‰}$  (e.g., Morin et al., 2022; Liu et al., 2022; Kawasaki et al., 2022; Nakamura et al., 2022), consistent with an average  $\Delta^{17}\text{O}$  of  $\leq -2\text{‰}$ . However, the majority of anhydrous solids accreted to the Ryugu parent body could have been amorphous silicate, such as GEMS (glass with embedded metal and sulfide)-like objects described in Ryugu by Nakamura et al. (2023) or those in other carbonaceous chondrites (e.g., Leroux et al., 2015; Ohtaki et al., 2021; Villalon et al., 2021). Oxygen isotope ratios of such GEMS-like objects are not known, because they are too small ( $\leq 1\ \mu\text{m}$ ) to be analyzed by SIMS at  $\text{‰}$  precisions. Even if they could be analyzed, their oxygen isotope

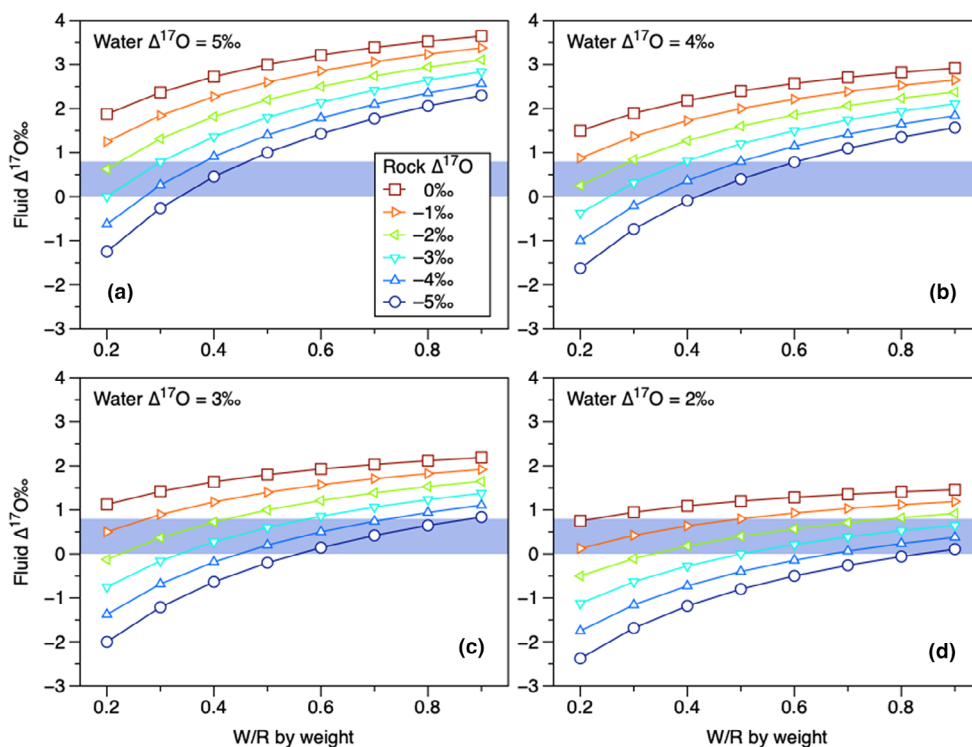


FIGURE 9. Estimation of  $\Delta^{17}\text{O}$  in aqueous fluid in more-altered conditions as a function of W/R (0.2–0.9), initial  $\Delta^{17}\text{O}$  in anhydrous solid ( $-5\text{‰}$  to  $0\text{‰}$ ), and the initial  $\Delta^{17}\text{O}$  of water (a:  $+5\text{‰}$ , b:  $+4\text{‰}$ , c:  $+3\text{‰}$ , and d:  $+2\text{‰}$ ). Shaded areas indicate the range of  $\Delta^{17}\text{O}$  observed from dolomite and breunnerite determined in this study. Parameters used are listed in Table S7.

ratios could be easily modified by the isotope exchange with aqueous fluid. It is possible that water ice and anhydrous silicate accreted to Ryugu parent body initially had distinct  $\Delta^{17}\text{O}$ ,  $>+2\text{‰}$  and  $<-2\text{‰}$ , respectively. At the early stage of aqueous alteration, interaction between aqueous fluid and amorphous silicate might have modified the  $\Delta^{17}\text{O}$  of fluid and solids to be  $\sim +2\text{‰}$  and  $\sim -2\text{‰}$ , respectively. As a result, aqueous fluid that formed in more-altered conditions had a smaller range of  $\Delta^{17}\text{O}$  close to bulk Ryugu, even with a large range of W/R.

At the low temperatures ( $0\text{--}20^\circ\text{C}$ ), magnetite does not fractionate significantly from water ( $1.7\text{‰}$  to  $-0.7\text{‰}$  in  $\delta^{18}\text{O}$ ; Hayles et al., 2018). If oxygen isotope ratios of spherulitic magnetite ( $\delta^{18}\text{O} \sim +5\text{‰}$ ,  $\Delta^{17}\text{O} \sim 2\text{‰}$ ) were in equilibrium with water, they are very close to the oxygen 3-isotope ratios of aqueous fluid at the early stage (point A in Figure 8). As discussed earlier, magnetite from pyrrhotite–dolomite–magnetite assemblage in A0058–C1002 ( $\delta^{18}\text{O} \sim -3\text{‰}$ ,  $\Delta^{17}\text{O} \sim 0.3\text{‰}$ ) might have formed at higher temperatures of  $40\text{--}80^\circ\text{C}$ , at which temperatures magnetite–water isotope fractionation factors are  $-3\text{‰}$  to  $-5\text{‰}$  in  $\delta^{18}\text{O}$ . The oxygen isotope ratios in the fluid are estimated to be  $\delta^{18}\text{O} \sim +1\text{‰}$  and  $\Delta^{17}\text{O} \sim 0.3\text{‰}$  (point B in Figure 8). This composition is nearly the same as those estimated by Yokoyama et al. (2023) from the same

Ryugu specimen (point C in Figure 8). These estimated fluid compositions are fractionated from the PCM line by  $\sim -5\text{‰}$  as shown in Figure 8. Furthermore, the composition of water in equilibrium with magnetite and dolomite pairs in C0002–C1001 from Nagashima et al. (2022) is estimated to be  $\delta^{18}\text{O} \sim +8\text{‰}$  and  $\Delta^{17}\text{O} \sim 0.6\text{‰}$  by applying the temperature of  $92^\circ\text{C}$  (point D in Figure 8), which is on the PCM line.

We could not apply oxygen isotope thermometry to breunnerite because we did not find a magnetite–breunnerite pair. However, systematically lower  $\delta^{18}\text{O}$  in coarse-grained breunnerite ( $\sim 21\text{‰}$ ) than dolomite may suggest that breunnerite formed under higher W/R and at higher temperatures than the majority of altered lithologies found in Ryugu samples. If the composition of fluid was similar to those estimated for A0058–C1001 magnetite ( $\delta^{18}\text{O} \sim +1\text{‰}$  and  $\Delta^{17}\text{O} \sim 0.3\text{‰}$ ), then the breunnerite–water isotope fractionation of  $\sim 20\text{‰}$  corresponds to the temperature of  $90\text{--}100^\circ\text{C}$ .

Alternatively, the lower  $\delta^{18}\text{O}$  of breunnerite could be caused by a fluid with fractionated  $\delta^{18}\text{O}$  due to a large amount of carbonate and phyllosilicate that have higher  $\delta^{18}\text{O}$ . Similarly, several euhedral magnetite grains in C0002 show high  $\Delta^{17}\text{O}$  of  $2\text{‰}$ , similar to spherulitic magnetite, but have significantly lower  $\delta^{18}\text{O}$  (from  $-4\text{‰}$  to  $0.6\text{‰}$ ). If they formed from the fluid with the same isotope ratios as

those for spherulitic magnetite, the formation temperature of these magnetite grains could be significantly high  $\geq 100^\circ\text{C}$ . However, aqueous fluid could have been fractionated to lower  $\delta^{18}\text{O}$  and produced magnetite that shows relatively lower  $\delta^{18}\text{O}$ . Thus, without having an equilibrium pair to which we can apply oxygen isotope thermometry, it is not easy to deliver reliable estimates of the temperatures and isotope ratios of aqueous fluid during the formation of altered minerals.

Fujiya et al. (2023) suggested that dolomite formed during retrograde cooling of the parent body when the aqueous fluid and silicate approached isotope equilibrium. If breunnerite with a lower  $\delta^{18}\text{O}$  than dolomite formed at a higher temperature than dolomite during the retrograde cooling, the formation of breunnerite would predate the formation of dolomite. Ryugu sample C0002-C1001, which we examined in this study, does not show any textural relationship between breunnerite and dolomite that indicates the crystallization sequence between them. In future studies, it would be useful to conduct a coordinate study between petrology and oxygen isotopes of altered minerals in Ryugu, which would provide us with a better understanding of fluid activity in the Ryugu parent asteroid.

### Comparison to CM and CR Chondrites

Oxygen isotope studies of aqueously altered minerals have been extensively investigated for CM and CR chondrites. Ca-carbonates (calcite and aragonite) are more abundant than other carbonates and magnetite in CM chondrites, so that oxygen and carbon isotope analyses of Ca-carbonate has been conducted using multiple analytical approaches; phosphoric acid dissolution to selectively dissolve calcite (and dolomite) from bulk powders (Alexander et al., 2015; Benedix et al., 2003; Clayton & Mayeda, 1984; Grady et al., 1988; Tyra et al., 2007), in situ SIMS analyses of Ca-carbonate on polished sections (Fujiya et al., 2015; Jenniskens et al., 2012; Lee et al., 2013; Telus et al., 2019; Tyra et al., 2012, 2016; Vacher et al., 2016, 2017, 2018, 2019; Verdier-Paoletti et al., 2017, 2019), and application of Clumped-isotope thermometry (Clog et al., 2024; Guo & Eiler, 2007). Calcite in CM chondrites shows a wide range of  $\delta^{18}\text{O}$  and  $\Delta^{17}\text{O}$ , typically from 15‰ to 40‰ and  $-4\text{‰}$  to  $+5\text{‰}$ , respectively. Several studies indicate correlation between oxygen isotope ratios and degrees of alterations, such as mineralogic alteration index (MAI; Benedix et al., 2003) and mineralogy, chemistry, and morphology of Ca-carbonate (Lee et al., 2013; Telus et al., 2019; Tyra et al., 2012; Vacher et al., 2017, 2018, 2019), suggesting that fluid started from higher  $\delta^{18}\text{O}$  and  $\Delta^{17}\text{O}$  values and evolved to lower values, similar to the case for Ryugu and CI chondrite parent bodies discussed above.

Guo and Eiler (2007) applied clumped-isotope thermometry to Ca-carbonate and estimated the fluid temperatures of three CM chondrites: 20–35°C for Murchison and Murray and  $\sim 71^\circ\text{C}$  for Cold Bokkeveld. In highly altered CM chondrites, ALH 83100, Telus et al. (2019) found consistent  $\Delta^{17}\text{O}$  values from dolomite and magnetite and an estimated dolomite–magnetite equilibrium temperature of  $125 \pm 60^\circ\text{C}$ . They are within a similar range of magnetite–dolomite equilibrium temperatures estimated for Ryugu A0058 in this study. More recently, Clog et al. (2024) applied clumped-isotope thermometry for several CM chondrites and determined a range of temperatures 5–51°C for calcite ( $\pm 10^\circ\text{C}$ ) and 75–101°C for dolomite ( $\pm 15^\circ\text{C}$ ). They further found a correlation between the estimated temperatures and  $\Delta^{17}\text{O}$ , which decrease from  $-1\text{‰}$  to  $-2.6\text{‰}$  with increasing temperatures. Jilly-Rehak et al. (2018) studied magnetite, calcite, and dolomite in CR chondrites with various alteration degrees. They found magnetite and carbonate plots along two parallel linear trends with the slopes of  $0.64 \pm 0.04$  and  $0.63 \pm 0.05$ , respectively, while having a systematic difference in  $\delta^{18}\text{O}$  that corresponds to the equilibrium temperatures between  $\sim 55$  and  $88^\circ\text{C}$ . Similarly, Verdier-Paoletti et al. (2017) suggested that CM calcite data plot on a single trend with the slope of  $0.66 \pm 0.05$  that extends to bulk CM chondrite data. They further estimated calcite precipitation temperatures by estimating the evolution trend of aqueous fluid to be 50–300°C (mean of  $110^\circ\text{C}$ ). Alexander et al. (2015) used oxygen and carbon isotope fractionation in calcite and dolomite in CM and CI chondrites and estimated precipitation temperatures of 0–130°C and 10–40°C, respectively. Clog et al. (2024) argued that temperatures estimated from geochemical modeling (e.g., Alexander et al., 2015; Verdier-Paoletti et al., 2017) are somewhat higher than those estimated by clumped-isotope thermometry.

In comparison to above CM and CR chondrite studies, we estimated the best fit line for magnetite data for Ryugu and found a similar slope of  $\sim 0.7$  (Figure S5) to those estimated for CM and CR chondrite magnetite and carbonate data. However, it is clear from the Figure 8 that carbonate data in Ryugu and CI chondrite would not plot on a single trend, as most carbonate data show a narrow range of  $\Delta^{17}\text{O}$  with a range of  $\delta^{18}\text{O}$ , except for some calcite data with highest  $\delta^{18}\text{O}$  and  $\Delta^{17}\text{O}$ . It is possible that magnetite and calcite show a similar slope by co-precipitated from a common fluid at relatively lower temperatures, similar to calcite and magnetite data found in CR and CM chondrites. Majority of carbonate show a narrow range of  $\Delta^{17}\text{O}$  and plot nearly along the slope 0.52 line along with some magnetite data in Ryugu and CI chondrites. Similar results have been obtained for magnetite and dolomite in



highly altered CR chondrite GRO 95577 (Jilly-Rehak et al., 2018) and CM chondrite ALH 83100 (Telus et al., 2019), which show indistinguishable  $\Delta^{17}\text{O}$  analyses between magnetite and carbonates.

## CONCLUSIONS

We performed SIMS oxygen 3-isotope analyses of magnetite, dolomite, and breunnerite in two sections of Ryugu samples, A0058 and C0002. Oxygen isotope ratios of magnetite correlate with their morphologies. Spherulitic magnetite shows consistently higher  $\delta^{18}\text{O}$  and  $\Delta^{17}\text{O}$  ( $\sim 2\text{‰}$ ) than euhedral magnetite with lower  $\delta^{18}\text{O}$  and variable  $\Delta^{17}\text{O}$  ( $0\text{--}2\text{‰}$ ). Oxygen isotope analyses of dolomite and breunnerite show a narrow range of  $\Delta^{17}\text{O}$  from  $0.0\text{‰}$  to  $0.8\text{‰}$ , similar to bulk oxygen isotope ratios. The majority of breunnerite, including large  $\geq 100\ \mu\text{m}$  grains, show systematically lower  $\delta^{18}\text{O}$  than dolomite, indicating that they did not form in isotope equilibrium. Magnetite and dolomite in coarse-grained lithology in A0058-C1002 show indistinguishable  $\Delta^{17}\text{O}$  (mean values and 2SD of  $0.30 \pm 0.60\text{‰}$  and  $0.18 \pm 0.29\text{‰}$ , respectively). The equilibrium temperatures between the mineral pair are estimated to be  $51 \pm 10^\circ\text{C}$  or  $77 \pm 12^\circ\text{C}$ , depending on the instrumental bias correction schemes for dolomite. A reliable temperature estimate requires a Mn-bearing dolomite standard to evaluate the instrumental bias corrections, which is not currently available.

These results indicate that the oxygen isotope ratios of aqueous fluids in the Ryugu parent asteroid were isotopically heterogeneous, spatially, and/or temporary. Under less-altered conditions, aqueous fluid had  $\Delta^{17}\text{O}$  of  $2\text{‰}$ , which are likely to be the lower limit of  $\Delta^{17}\text{O}$  of water ice that accreted to the parent body. The  $\Delta^{17}\text{O}$  of fluid would become lower and close to that of bulk by extensive water–rock interactions. The  $\delta^{18}\text{O}$  of carbonate from this study and literature tend to decrease in the order of calcite, dolomite, and breunnerite, which is the same order of increasing W/R of the aqueous alteration. The systematic changes of  $\delta^{18}\text{O}$  may be related to an increase of temperatures with the degrees of aqueous alteration. Alternatively, the  $\delta^{18}\text{O}$  value of fluid would be shifted to lower values under the more-altered conditions because of abundant carbonate and phyllosilicates that enrich heavy oxygen isotopes relative to water. Without having a suitable mineral pair that we can apply oxygen isotope thermometry to, the isotope ratios and temperatures of the aqueous fluid would not be estimated independently.

*Acknowledgments*—This work is carried out under the Hayabusa2 Initial Analysis Team, specifically the Chemistry subteam led by H. Yurimoto. We thank assistance by Bil Schneider for SEM and Michael Spicuzza for SIMS

instruments. Authors thank constructive reviews by anonymous reviewers and editorial handling by Yves Marrocchi. This work is supported by NASA (80NSS C20K0486: NK), and WiscSIMS laboratory is funded by NSF-EAR (EAR-2004618).

*Data Availability Statement*—The data that support the findings of this study are available in the supplementary material of this article, and additional data are openly available in Dryad Digital Repository at <http://doi.org/10.5061/dryad.dv41ns246>.

*Editorial Handling*—Dr. Yves Marrocchi

## REFERENCES

- Aléon, J., Mostefaoui, S., Bureau, H., Vangu, D., Khodja, H., Nagashima, K., Kawasaki, N., et al. 2024. Hydrogen in Magnetite from Asteroid Ryugu. *Meteoritics & Planetary Science* (in press). <https://doi.org/10.1111/maps.14139>.
- Alexander, C. M. O'D., Bowden, R., Fogel, M. L., and Howard, K. T. 2015. Carbonate Abundances and Isotopic Compositions in Chondrites. *Meteoritics & Planetary Science* 50: 810–833.
- Alfing, J., Patzek, M., and Bischoff, A. 2019. Modal Abundances of Coarse-Grained ( $>5\ \mu\text{m}$ ) Components within CI-Chondrites and their Individual Clasts—Mixing of Various Lithologies on the CI Parent Body(ies). *Geochemistry* 79: 125532.
- Baertschi, P. 1976. Absolute  $^{18}\text{O}$  Content of Standard Mean Ocean Water. *Earth and Planetary Science Letters* 31: 341–44.
- Batchelor, C. J., Marcott, S. A., Orland, I. J., and Kitajima, K. 2022. Late Holocene Increase of Winter Precipitation in Mid-Continental North America from a Seasonally Resolved Speleothem Record. *Geology* 50: 781–85.
- Benedix, G. K., Leshin, L. A., Farquhar, J., Jackson, T., and Thiemens, M. H. 2003. Carbonates in CM2 Chondrites: Constraints on Alteration Conditions from Oxygen Isotopic Compositions and Petrographic Observations. *Geochimica et Cosmochimica Acta* 67: 1577–88.
- Bouden, N., Villeneuve, J., Marrocchi, Y., Deloule, E., Füre, E., Gurenko, A., Piani, L., Thomassot, E., Peres, P., and Fernandes, F. 2021. Triple Oxygen Isotope Measurements by Multi-Collector Secondary Ion Mass Spectrometry. *Frontiers in Earth Science* 8: 601169.
- Clayton, R. N., and Mayeda, T. K. 1984. The Oxygen Isotope Record in Murchison and Other Carbonaceous Chondrites. *Earth and Planetary Science Letters* 67: 151–161.
- Clayton, R. N., Mayeda, T. K., Goswami, J. N., and Olsen, E. J. 1991. Oxygen Isotope Studies of Ordinary Chondrites. *Geochimica et Cosmochimica Acta* 55: 2317–37.
- Clog, M., Lindgren, P., Modestou, S., McDonald, A., Tait, A., Donnelly, T., Mark, D., and Lee, M. 2024. Clumped Isotope and  $\Delta^{17}\text{O}$  Measurements of Carbonates in CM Carbonaceous Chondrites: New Insights into Parent Body Thermal and Fluid Evolution. *Geochimica et Cosmochimica Acta* 369: 1–16.
- Dobrică, E., Ishii, H. A., Bradley, J. P., Ohtaki, K., Brearley, A. J., Noguchi, T., Matsumoto, T., et al. 2023. Nonequilibrium Spherulitic Magnetite in the Ryugu Samples. *Geochimica et Cosmochimica Acta* 346: 65–75.

- Fujiya, W., Kawasaki, N., Nagashima, K., Sakamoto, N., Alexander, C. M. O'D., Kita, N. T., Kitajima, K., et al. 2023. Carbonate Record of the Change in Oxygen Fugacity and Gaseous Species in Asteroid Ryugu. *Nature Geoscience* 16: 675–682.
- Fujiya, W., Sugiura, N., Marrocchi, Y., Takahata, N., Hoppe, P., Shirai, K., Sano, Y., and Hiyagon, H. 2015. Comprehensive Study of Carbon and Oxygen Isotopic Compositions, Trace Element Abundances, and Cathodoluminescence Intensities of Calcite in the Murchison CM Chondrite. *Geochimica et Cosmochimica Acta* 161: 101–117.
- Fukuda, K., Brownlee, D. E., Joswiak, D. J., Tenner, T. J., Kimura, M., and Kita, N. T. 2021. Correlated Isotopic and Chemical Evidence for Condensation Origins of Olivine in Comet 81P/Wild 2 and in AOAs from CV and CO Chondrites. *Geochimica et Cosmochimica Acta* 293: 544–574.
- Fukuda, K., Tenner, T. J., Kimura, M., Tomioka, N., Siron, G., Ushikubo, T., Chaumard, N., Hertwig, A. T., and Kita, N. T. 2022. A Temporal Shift of Chondrule Generation from the Inner to Outer Solar System Inferred from Oxygen Isotopes and Al-Mg Chronology of Chondrules from Primitive CM and CO Chondrites. *Geochimica et Cosmochimica Acta* 322: 194–226.
- Grady, M. M., Wright, I. P., Swart, P. K., and Pillinger, C. T. 1988. The Carbon and Oxygen Isotopic Composition of Meteoritic Carbonates. *Geochimica et Cosmochimica Acta* 52: 2855–66.
- Greenwood, R. C., Franchi, I. A., Findlay, R., Malley, J. A., Ito, M., Yamaguchi, A., Kimura, M., et al. 2022. Oxygen Isotope Evidence from Ryugu Samples for Early Water Delivery to Earth by CI Chondrites. *Nature Astronomy* 7: 29–38.
- Guo, W., and Eiler, J. M. 2007. Temperatures of Aqueous Alteration and Evidence for Methane Generation on the Parent Bodies of the CM Chondrites. *Geochimica et Cosmochimica Acta* 71: 5565–75.
- Hayles, J., Gao, C., Cao, X., Liu, Y., and Bao, H. 2018. Theoretical Calibration of the Triple Oxygen Isotope Thermometer. *Geochimica et Cosmochimica Acta* 235: 237–245.
- Huberty, J. M., Kita, N. T., Kozdon, R., Heck, P. R., Fournelle, J. H., Spicuzza, M. J., Xu, H., and Valley, J. W. 2010. Crystal Orientation Effects in  $\delta^{18}\text{O}$  for Magnetite and Hematite by SIMS. *Chemical Geology* 276: 269–283.
- Ito, M., Tomioka, N., Uesugi, M., Yamaguchi, A., Shirai, N., Ohigashi, T., Liu, M.-C., et al. 2022. A Pristine Record of Outer Solar System Materials from Asteroid Ryugu's Returned Sample. *Nature Astronomy* 6: 1163–71.
- Jenniskens, P., Fries, M. D., Yin, Q.-Z., Zolensky, M., Krot, A. N., Sandford, S. A., Sears, D., et al. 2012. Radar-Enabled Recovery of the Sutter's Mill Meteorite, a Carbonaceous Chondrite Regolith Breccia. *Science* 338: 1583–87.
- Jilly-Rehak, C. E., Huss, G. R., Nagashima, K., and Schrader, D. L. 2018. Low-Temperature Aqueous Alteration on the CR Chondrite Parent Body: Implications from In Situ Oxygen-Isotope Analyses. *Geochimica et Cosmochimica Acta* 222: 230–252.
- Kawasaki, N., Nagashima, K., Sakamoto, N., Matsumoto, T., Bajo, K., Wada, S., Igami, Y., et al. 2022. Oxygen Isotopes of Anhydrous Primary Minerals show Kinship between Asteroid Ryugu and Comet 81P/Wild2. *Science Advances* 8: eade2067.
- Kimura, J.-I., Chang, Q., Kanazawa, N., Sasaki, S., and Vaglarov, B. S. 2016. High-Precision In Situ Analysis of Pb Isotopes in Glasses Using  $10^{13} \Omega$  Resistor High Gain Amplifiers with Ultraviolet Femtosecond Laser Ablation Multiple Faraday Collector Inductively Coupled Plasma Mass Spectrometry. *Journal of Analytical Atomic Spectrometry* 31: 790–800.
- Kita, N. T., Sobol, P. E., Kern, J. R., Lord, N. E., and Valley, J. W. 2015. UV-Light Microscope: Improvements in Optical Imaging for a Secondary Ion Mass Spectrometer. *Journal of Analytical Atomic Spectrometry* 30: 1207–13.
- Kita, N. T., Ushikubo, T., Fu, B., and Valley, J. W. 2009. High precision SIMS oxygen isotope analysis and the effect of sample topography. *Chemical Geology* 264(1–4): 43–57. <https://doi.org/10.1016/j.chemgeo.2009.02.012>.
- Kozdon, R., Ushikubo, T., Kita, N. T., Spicuzza, M., and Valley, J. W. 2009. Intratest Oxygen Isotope Variability in the Planktonic Foraminifer *N. Pachyderma*: Real vs. Apparent Vital Effects by Ion Microprobe. *Chemical Geology* 258: 327–337.
- Lee, M. R., Sofe, M. R., Lindgren, P., Starkey, N. A., and Franchi, I. A. 2013. The Oxygen Isotope Evolution of Parent Body Aqueous Solutions as Recorded by Multiple Carbonate Generations in the Lonewolf Nunataks 94101 CM2 Carbonaceous Chondrite. *Geochimica et Cosmochimica Acta* 121: 452–466.
- Leroux, H., Cuvillier, P., Zanda, B., and Hewins, R. H. 2015. GEMS-Like Material in the Matrix of the Paris Meteorite and the Early Stages of Alteration of CM Chondrites. *Geochimica et Cosmochimica Acta* 170: 247–265.
- Linzmeier, B., Kitajima, K., Denny, A., and Cammack, J. 2018. Making Maps on a Micrometer Scale. *Eos* 99. <https://doi.org/10.1029/2018EO099269>.
- Liu, M.-C., McCain, K. A., Matsuda, N., Yamaguchi, A., Kimura, M., Tomioka, N., Ito, M., et al. 2022. Incorporation of  $^{16}\text{O}$ -Rich Anhydrous Silicates in the Protolith of Highly Hydrated Asteroid Ryugu. *Nature Astronomy* 6: 1172–77.
- McCain, K. A., Matsuda, N., Liu, M.-C., McKeegan, K. D., Yamaguchi, A., Kimura, M., Tomioka, N., et al. 2023. Early Fluid Activity on Ryugu Inferred by Isotopic Analyses of Carbonates and Magnetite. *Nature Astronomy* 7: 309–317.
- Morin, G. L. F., Marrocchi, Y., Villeneuve, J., and Jacquet, E. 2022.  $^{16}\text{O}$ -Rich Anhydrous Silicates in CI Chondrites: Implications for the Nature and Dynamics of Dust in the Solar Accretion Disk. *Geochimica et Cosmochimica Acta* 332: 203–219.
- Nagashima, K., Kawasaki, N., Sakamoto, N., Fujiya, W., Yurimoto, H., and The Hayabusa2-Initial-Analysis Chemistry Team, and the Hayabusa2-Initial-Analysis Core. 2022. Distinct Ages and Temperatures of Aqueous Activities Recorded in Ryugu Samples (Abstract). Hayabusa Symposium.
- Nakamura, E., Kobayashi, K., Tanaka, R., Kunihiro, T., Kitagawa, H., Potiszil, C., Ota, T., et al. 2022. On the Origin and Evolution of the Asteroid Ryugu: A Comprehensive Geochemical Perspective. *Proceedings of the Japan Academy, Series B* 98: 227–282.
- Nakamura, T., Matsumoto, M., Amano, K., Enokido, Y., Zolensky, M. E., Mikouchi, T., Genda, H., et al. 2023. Formation and Evolution of Carbonaceous Asteroid Ryugu: Direct Evidence from Returned Samples. *Science* 379: eabn8671.

- Nakashima, D., Nakamura, T., Zhang, M., Kita, N. T., Mikouchi, T., Yoshida, H., Enokido, Y., et al. 2023. Chondrule-Like Objects and Ca-Al-Rich Inclusions in Ryugu May Potentially be the Oldest Solar System Materials. *Nature Communications* 14: 532.
- Ohtaki, K. K., Ishii, H. A., Bradley, J. P., Villalon, K. L., Davis, A. M., Stephan, T., Bustillo, K. C., and Ciston, J. 2021. Search for Meteoritic GEMS I: Comparison of Amorphous Silicates in Paris and Acfer 094 Chondrite Matrices and in Anhydrous Chondritic Interplanetary Dust Particles. *Geochimica et Cosmochimica Acta* 310: 320–345.
- Piralla, M., Marrocchi, Y., Verdier-Paoletti, M. J., Vacher, L. G., Villeneuve, J., Piani, L., Bekaert, D. V., and Gounelle, M. 2020. Primordial Water and Dust of the Solar System: Insights from In Situ Oxygen Measurements of CI Chondrites. *Geochimica et Cosmochimica Acta* 269: 451–464.
- Rowe, M. W., Clayton, R. N., and Mayeda, T. K. 1994. Oxygen Isotopes in Separated Components of CI and CM Meteorites. *Geochimica et Cosmochimica Acta* 58: 5341–47.
- Siron, G., Fukuda, K., Kimura, M., and Kita, N. T. 2021. New Constraints from  $^{26}\text{Al}$ - $^{26}\text{Mg}$  Chronology of Anorthite Bearing Chondrules in Unequilibrated Ordinary Chondrites. *Geochimica et Cosmochimica Acta* 293: 103–126.
- Siron, G., Fukuda, K., Kimura, M., and Kita, N. T. 2022. High Precision  $^{26}\text{Al}$ - $^{26}\text{Mg}$  Chronology of Chondrules in Unequilibrated Ordinary Chondrites: Evidence for Restricted Formation Ages. *Geochimica et Cosmochimica Acta* 324: 312–345.
- Śliwiński, M. G., Kitajima, K., Kozdon, R., Spicuzza, M. J., Fournelle, J. H., Denny, A., and Valley, J. W. 2016. Secondary Ion Mass Spectrometry Bias on Isotope Ratios in Dolomite-Ankerite, Part II:  $\delta^{13}\text{C}$  Matrix Effects. *Geostandards and Geoanalytical Research* 40: 173–184.
- Śliwiński, M. G., Kitajima, K., Spicuzza, M. J., Orland, I. J., Ishida, A., Fournelle, J. H., and Valley, J. W. 2018. SIMS Bias on Isotope Ratios in Ca-Mg-Fe Carbonates (Part III):  $\delta^{18}\text{O}$  and  $\delta^{13}\text{C}$  Matrix Effects along the Magnesite-Siderite Solid-Solution Series. *Geostandards and Geoanalytical Research* 42: 49–76.
- Tachibana, S., Sawada, H., Okazaki, R., Takano, Y., Sakamoto, K., Miura, Y. N., Okamoto, C., et al. 2022. Pebbles and Sand on Asteroid (162173) Ryugu: In Situ Observation and Particles Returned to Earth. *Science* 375: 1011–16.
- Telus, M., Alexander, C. M. O'D., Hauri, E. H., and Wang, J. 2019. Calcite and Dolomite Formation in the CM Parent Body: Insight from In Situ C and O Isotope Analyses. *Geochimica et Cosmochimica Acta* 260: 275–291.
- Tsuchiyama, A., Matsumoto, M., Matsuno, J., Nakamura, T., Noguchi, T., Yasutake, M., Uesugi, K., et al. 2022. 3D Morphologies of Magnetite, Sulfides, Carbonates and Phosphates in Ryugu Samples and their Crystallization Sequence during Aqueous Alteration (abstract). *Meteoritics & Planetary Science* 57(Suppl.):6221.pdf.
- Tyra, M., Brearley, A., and Guan, Y. 2016. Episodic Carbonate Precipitation in the CM Chondrite ALH 84049: An Ion Microprobe Analysis of O and C Isotopes. *Geochimica et Cosmochimica Acta* 175: 195–207.
- Tyra, M. A., Farquhar, J., Guan, Y., and Leshin, L. A. 2012. An Oxygen Isotope Dichotomy in CM2 Chondritic Carbonates—A SIMS Approach. *Geochimica et Cosmochimica Acta* 77: 383–395.
- Tyra, M. A., Farquhar, J., Wing, B. A., Benedix, G. K., Jull, A. J. T., Jackson, T., and Thiemens, M. H. 2007. Terrestrial Alteration of Carbonate in a Suite of Antarctic CM Chondrites: Evidence from Oxygen and Carbon Isotopes. *Geochimica et Cosmochimica Acta* 71: 782–795.
- Ushikubo, T., Kimura, M., Kita, N. T., and Valley, J. W. 2012. Primordial Oxygen Isotope Reservoirs of the Solar Nebula Recorded in Chondrules in Acfer 094 Carbonaceous Chondrite. *Geochimica et Cosmochimica Acta* 90: 242–264.
- Vacher, L. G., Marrocchi, Y., Verdier-Paoletti, M. J., Villeneuve, J., and Gounelle, M. 2016. Inward Radial Mixing of Interstellar Water Ices in the Solar Protoplanetary Disk. *The Astrophysical Journal Letters* 827: L1.
- Vacher, L. G., Marrocchi, Y., Villeneuve, J., Verdier-Paoletti, M. J., and Gounelle, M. 2017. Petrographic and C & O Isotopic Characteristics of the Earliest Stages of Aqueous Alteration of CM Chondrites. *Geochimica et Cosmochimica Acta* 213: 271–290.
- Vacher, L. G., Marrocchi, Y., Villeneuve, J., Verdier-Paoletti, M. J., and Gounelle, M. 2018. Collisional and Alteration History of the CM Parent Body. *Geochimica et Cosmochimica Acta* 239: 213–234.
- Vacher, L. G., Piralla, M., Gounelle, M., Bizzarro, M., and Marrocchi, Y. 2019. Thermal Evolution of Hydrated Asteroids Inferred from Oxygen Isotopes. *The Astrophysical Journal* 882: L20.
- Verdier-Paoletti, M. J., Marrocchi, Y., Avice, G., Roskosz, M., Gurenko, A., and Gounelle, M. 2017. Oxygen Isotope Constraints on the Alteration Temperatures of CM Chondrites. *Earth and Planetary Science Letters* 458: 273–281.
- Verdier-Paoletti, M. J., Marrocchi, Y., Vacher, L. G., Gattacceca, J., Gurenko, A., Sonzogni, C., and Gounelle, M. 2019. Testing the Genetic Relationship between Fluid Alteration and Brecciation in CM Chondrites. *Meteoritics & Planetary Science* 54: 1692–1709.
- Villalon, K. L., Ohtaki, K. K., Bradley, J. P., Ishii, H. A., Davis, A. M., and Stephan, T. 2021. Search for Meteoritic GEMS II: Comparison of Inclusions in Amorphous Silicates from the Paris Chondrite and from Anhydrous Chondritic Interplanetary Dust Particles. *Geochimica et Cosmochimica Acta* 310: 346–362.
- Watanabe, S., Hirabayashi, M., Hirata, N., Hirata, N., Noguchi, R., Shimaki, Y., Ikeda, H., et al. 2019. Hayabusa2 Arrives at the Carbonaceous Asteroid 162173 Ryugu—A Spinning Top-Shaped Rubble Pile. *Science* 364: 268–272.
- Yamaguchi, A., Tomioka, N., Ito, M., Shirai, N., Kimura, M., Greenwood, R. C., Liu, M.-C., et al. 2023. Insight into Multi-Step Geological Evolution of C-Type Asteroids from Ryugu Particles. *Nature Astronomy* 7: 398–405.
- Yokoyama, T., Nagashima, K., Nakai, I., Young, E. D., Abe, Y., Aléon, J., Alexander, C. M. O'D., et al. 2023. Samples Returned from the Asteroid Ryugu are Similar to Ivuna-Type Carbonaceous Meteorites. *Science* 379: eabn7850.
- Young, E. D., Kohl, I. E., Warren, P. H., Rubie, D. C., Jacobson, S. A., and Morbidelli, A. 2016. Oxygen Isotopic Evidence for Vigorous Mixing during the Moon-Forming Giant Impact. *Science* 351: 493–96.

- Zhang, M., Fukuda, K., Spicuzza, M. J., Siron, G., Heimann, A., Hammerstrom, A. J., Kita, N. T., Ushikubo, T., and Valley, J. W. 2022. SIMS Matrix Effects in Oxygen Isotope Analysis of Olivine and Pyroxene: Application to Acfer 094 Chondrite Chondrules and Reconsideration of the Primitive Chondrule Minerals (PCM) Line. *Chemical Geology* 608: 121016.
- Zheng, Y. 1991. Calculation of Oxygen Isotope Fractionation in Metal Oxides. *Geochimica et Cosmochimica Acta* 55: 2299–2307.
- Zheng, Y.-F. 1999. Oxygen Isotope Fractionation in Carbonate and Sulfate Minerals. *Geochemical Journal* 33: 109–126.

## SUPPORTING INFORMATION

Additional supporting information may be found in the online version of this article.

**Table S1.** Composition of carbonate estimated from EDS analyses.

**Table S2.** Raw SIMS oxygen isotope data for carbonate analyses session.

**Table S3.** Oxygen isotope analyses of magnetite standard and magnetite in Ryugu.

**Table S4.** Instrumental biases of carbonate standard.

**Table S5.** Instrumental bias-corrected oxygen isotope ratios for Ryugu carbonates.

**Table S6.** Oxygen isotope thermometry between carbonate and magnetite.

**Table S7.** Model estimate of  $\Delta^{17}\text{O}$  in an aqueous fluid.

**Figure S1.** X-ray map of the entire sections of A0058-C1002 and C0002-C1001.

**Figure S2.** Variation of  $\Delta^{17}\text{O}_{\text{RAW}}$  of carbonate standards relative to UWC-3 calcite standard. (a) Plot against Fe# of carbonate standards. (b) Plot against instrumental bias on  $\delta^{18}\text{O}$ .

**Figure S3.** Reproducibility of  $\delta^{18}\text{O}_{\text{RAW}}$  and  $\Delta^{17}\text{O}_{\text{RAW}}$  of randomly oriented grains of magnetite standard 5830. Data are shown with the analysis sequence.

**Figure S4.** Location of SIMS analyses and  $\delta^{18}\text{O}$  values of magnetite and dolomite from pyrrhotite–magnetite–dolomite assemblage in A0058-C1002. The  $\delta^{18}\text{O}$  values of dolomite are shown by using Fe# correction method.

**Figure S5.** Least square fit of magnetite oxygen isotope data. Data are same as those in Figure 5.